FFI-rapport 2015/00608

Modelling the elastic stiffness of nanocomposites using interphase models

Tom Thorvaldsen

FFI Forsvarets forskningsinstitutt

Modelling the elastic stiffness of nanocomposites using interphase models

Tom Thorvaldsen

Norwegian Defence Research Establishment (FFI)

15 June 2015

FFI-rapport 2015/00608

122701

P: ISBN 978-82-464-2550-4
E: ISBN 978-82-464-2551-1

Keywords

Matematiske modeller

Nanoteknologi

Partikler

Elastisitet

Kontinuumsmekanikk

Approved by

Rune Lausund	Project Manager
Jon E. Skjervold	Director

English summary

This report describes mathematical modelling of the elastic stiffness of *nanocomposites*, which in this context is referred to as particles of nano-size included in a polymer matrix, i.e. particles with one dimension of nanometre size. The main motivation for this work was to establish mathematical models for calculating the elastic properties of different nanocomposites, which then can be included in a "model toolbox" for future applications and for improved understanding of this type of materials. In this study, it is assumed that micromechanics models and continuum mechanics theory can be applied in the modelling.

In this report, an interphase model found in the literature is considered. The interphase is defined as the layer surrounding the particle, which has different elastic properties compared to the neat matrix (and the particle). Such models can thus be applied for describing changes in the polymer structure due to the inclusions, the bonding properties between the particle and the matrix, as well as the stiffness increase for the composite as a function of particle volume fraction.

Only spherical particles are included in the interphase model considered. Extensions of the model that include other spheroidal inclusion shapes than spheres are therefore presented. With the introduction of non-spherical inclusions, random orientation of the particles is also relevant. Stiffness expressions are presented for including randomly oriented spheroidal inclusions. The general two-phase Mori-Tanaka, described and analyzed in more detail in another recent FFI report, is included for comparison.

The composite elastic stiffness calculated by the interphase model and the two-phase Mori-Tanaka model is found to agree well for different spheroidal inclusion shapes and orientations.

The composite stiffness calculations from using the interphase model are also compared with experimental data for two different nanocomposites. Based on a very brief and initial analysis, the model calculations are observed to agree well with the experimental data. Hence, the significant stiffness increase for some composites, especially for low volume fractions, may be explained by interphase effects. A more thorough and detailed analysis than presented in this report can be found in a recent paper by the author (submitted to journal in March 2015).

Future studies should consider other factors that will influence the composite elastic stiffness, as well as other particles, such as graphene.

Sammendrag

Denne rapporten beskriver matematisk modellering av elastisk stivhet for nanokompositter, som i denne konteksten refererer til partikler av nanostørrelse som er inkludert i en polymermatrise, det vil si partikler der en av dimensjonene er i nanometer. Hovedmotivasjonen for dette arbeidet har vært å etablere matematiske modeller som kan benyttes for å beregne de elastiske egenskapene til ulike nanokompositter, som deretter kan inkluderes i en "modellverktøykasse" for fremtidige applikasjoner og for økt forståelse av denne typen materialer. Det er antatt at mikromekaniske modeller og kontinuummekanikk kan benyttes i modelleringen.

Denne rapporten tar for seg en interfasemodell som er funnet i litteraturen. Interfasen er definert som et lag som omkranser partikkelen, med andre elastiske egenskaper enn matrisen (og partikkelen). Slike modeller kan benyttes for å beskrive endringer i polymerstrukturen som følge av inklusjonene, heftegenskapene mellom partikkel og matrise, så vel som økningen i stivhet for kompositt som en funksjon av partikkelvolumfraksjon.

Det er kun sfæriske partikler som er inkludert i interfasemodellen. Utvidelser av modellen er derfor presentert, hvor også andre inklusjonsgeometrier ut over kuleformede er inkludert. Ved introduksjon av ikke-sfæriske partikler, er det også relevant å se på tilfeldig orientering av partikler. Uttrykk er derfor presentert, hvor vilkårlig orientering av partiklene er inkludert. Den generelle Mori-Tanaka-modellen, som er beskrevet og analysert in mer detalj i en annen FFI-rapport, er tatt med for sammenlikning.

Det er godt samsvar mellom den elastiske stivheten til kompositt beregnet ved bruk av interfasemodellen og to-fase Mori-Tanaka-modellen for ulike inklusjonsgeometrier og orienteringer.

Stivhetsberegningene for interfasemodellen er også sammenliknet med eksperimentelle data for to ulike nanokompositter. Basert på en generell og initiell analyse, er det observert at beregningene samsvarer bra med eksperimentelle data. Den betydelige stivhetsøkningen for noen kompositter, spesielt for små volumefraksjoner, kan derfor beskrives ved interfaseeffekter. En mer grundig og detaljert analyse enn det som er presentert i denne rapporten er gitt i en journalartikkel av forfatteren (innsendt til tidsskrift i mars 2015).

Fremtidige studier bør fokusere på andre faktorer som kan påvirke den elastiske stivheten til kompositt, så vel som andre partikler, slik som grafén.

Contents

1 Introduction

The work presented in this report is a follow-up study of the work by Thorvaldsen [1], where different models for the elastic stiffness of nanocomposites based on the Mori-Tanaka method were described. This study considered different two-phase models, which included specialized expressions for given particle/matrix systems with a given spheroidal shape and orientation, but also a more general model that can be applied for all spheroidal shaped inclusions (i.e. spheres, oblate and prolate shaped). A set of assumptions were made for the modelling. First of all, all particles have a spheroidal shape and are aligned or randomly oriented. All fibre-like inclusions were assumed straight, i.e. no waviness was included. Moreover, a full load transfer between the particles and the surrounding matrix was assumed. Finally, the particles were presumed to be perfectly dispersed in the matrix, i.e. no voids or agglomerates were present in the matrix. This latter assumption was the main reason for restricting to two-phase composites. Another follow-up study by Thorvaldsen opened for a second inclusion phase, i.e. three-phase models [2]. In this study, the same assumptions were made, except that a second inclusion phase, i.e. voids, agglomerates or other particles, was included in the model expressions. In both previous studies, the model results were compared with experimental results, and it was concluded that a multi-phase Mori-Tanaka based method, or other multi-phase models, may not be sufficient for describing all type of nanoparticle/polymer composites.

Studies have shown that the particle *interphase* should be taken into account when establishing models for nanocomposites, see e.g. [3;4]. The interphase is defined as the layer surrounding the particles, see Figure 1.1. Depending on the binding between the particles and the matrix, which may be modified and altered, for example by functionalization or other surface treatment to the particles, see e.g. [5], the elastic properties of the non-bulk interphase region will vary. For example, from a recent study by Hseih *et al.* [6] it seems that the curing agent in the polymer system will influence on the toughness of the composite. This could again indicate that the elastic stiffness of the interphase region is depending on the curing agent, which moreover will influence on the binding between the particles and the matrix. The elastic properties of the interphase are thus generally different from the neat matrix.

In this report, we consider mathematical models taking the particle interphase into account, and study and report how the interphase properties will affect the elastic stiffness of the nanocomposite. The study is restricted to one inclusion phase in the matrix. Hence, no voids or agglomerates are assumed to be present in the composite. This study is also restricted to the case of constant thickness of the interphase, i.e. no variation of the interphase thickness as a function of volume fraction of the particles. Extending the model analysis to also include a variation in interphase thickness may be relevant, but will then include tuning of two parameters, i.e. the elastic stiffness of the interphase and its thickness; a recently submitted journal paper includes the interphase thickness factor variation [7]. The interphase model results are compared with the calculated elastic stiffness using the general two-phase Mori-Tanaka model, which has been

found from the two previous studies to be the most flexible and applicable model. The interphase model results are furthermore compared with available experimental data found in the literature.

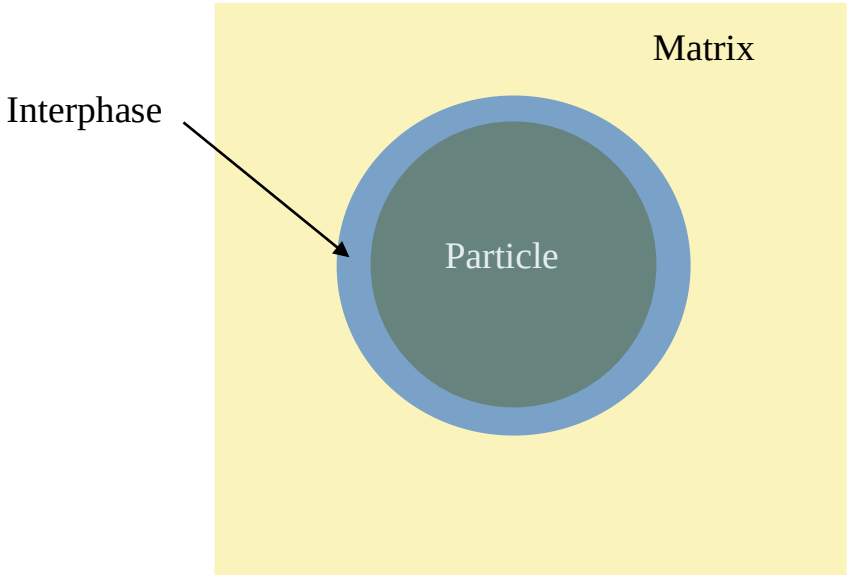

Figure 1.1 Representative volume entity for a nanoparticle. The particle is surrounded by an interphase region, with different elastic properties compared to the neat matrix.

2 Mathematical models

In this section, models that take into account the interphase region in nanoparticle/polymer composites are presented. The interphase model for aligned spherical inclusions is taken from the literature. Due to restrictions of this model, modifications/extensions that include non-spherical inclusions are also presented, as well as composites with randomly oriented inclusions.

For completeness and for comparison with the interphase models, the general Mori-Tanaka multi-phase model, described in the two previous studies [1;2], is included also in this report.

2.1 The general Mori-Tanaka model

The general Mori-Tanaka model for a multi-phase composite with *unidirectionally aligned inclusions* can be expressed as

$$\begin{aligned} C_C &= V_0 C_0 A_0 + \sum_{r=1}^{N-1} V_r C_r A_r \\ &= \left(V_0 C_0 + \sum_{r=1}^{N-1} V_r C_r A_r^{dil} \right) \left(V_0 I + \sum_{r=1}^{N-1} V_r A_r^{\mathrm{dil}} \right)^{-1} = \left(V_0 C_0 + \sum_{r=1}^{N-1} V_r C_r A_r^{dil} \right) A_0 \end{aligned} \tag{2.1}$$

where in the above expressions

$$A_r^{\text{dil}} = [I + S_r C_r^{-1}(C_0 - C_r)]^{-1} \tag{2.2}$$

$$A_0 = \left[V_0 I + \sum_{r=1}^{N-1} V_r A_r^{dil} \right]^{-1} \tag{2.3}$$

and

$$A_r = A_r^{\text{dil}} A_0 \tag{2.4}$$

For a two-phase composite, (2.1) this can be written as

$$C_C = \left(V_m C_m + V_p C_p A_p^{dil} \right) \left(V_m I + V_p A_p^{\text{dil}} \right)^{-1} \tag{2.5}$$

where m is the matrix phase and p the inclusion phase. Furthermore, V_m is the volume fraction of the matrix, V_p is the volume fraction of the inclusions, C_m is the stiffness matrix of the matrix, C_p is the stiffness matrix of the inclusions, I the identity matrix and

$$A_p^{\text{dil}} = [I + S_p C_p^{-1}(C_m - C_p)]^{-1} \tag{2.6}$$

where S_p is the Eshelby tensor for the inclusions [8;9]. Expressions for the Eshelby tensor for relevant inclusion geometries may be found in [1] and the references therein.

The general Mori-Tanaka model for a multi-phase composite with *randomly oriented inclusions* can in a similar way be expressed as

$$C_{C,random} = \left(V_0 C_0 + \sum_{r=1}^{N-1} V_r \{ C_r A_r^{dil} \} \right) \left(V_0 I + \sum_{r=1}^{N-1} V_r A_r^{\text{dil}} \right)^{-1} = \left(V_0 C_0 + \sum_{r=1}^{N-1} V_r \{ C_r A_r^{dil} \} \right) A_0 \tag{2.7}$$

where the curly brackets indicate orientationally averaging of all possible orientations, as described and showed in [3], and also [1]. The expression in (2.7) may for a two-phase composite be written as

$$C_C = \left(V_m C_m + V_p \left\{ C_p A_p^{dil} \right\} \right) \left(V_m I + V_p A_p^{\text{dil}} \right)^{-1} \tag{2.8}$$

2.2 The effective interphase model for spherical inclusions

An effective interphase model has been presented by Odegard *et al.* [10;11] for composites with spherical inclusions. This model includes an interphase surrounding the nanoparticle. Note that Odegard *et al.* refer to their model as an "effective interface model". To the author's knowledge and understanding, the *interface* is the surface of the particle being in contact with the non-bulk matrix. The *interphase,* on the other hand, is the non-bulk matrix region, with a certain thickness surrounding the particle. This latter terminology is also in accordance with Fisher and Brinson [3], and will thus be employed in this report.

A nanoparticle/polymer composite where the particles have a surrounding interphase region and a bulk matrix phase outside the interphase, can be expressed as,

$$C_C = C_m + \left[\left(V_p + V_i\right)\left(C_i - C_m\right)A_{pi} + V_p\left(C_p - C_i\right)A_p\right]\left[V_m I + \left(V_p + V_i\right)A_{pi}\right]^{-1} \qquad (2.9)$$

where in this case

$$A_p = I - S_p\left[S_p + (C_p - C_m)^{-1}C_m\right]^{-1} \qquad (2.10)$$

and

$$A_{pi} = I - S_p\left\{\frac{V_p}{V_i + V_p}\left[S_p + (C_p - C_m)^{-1}C_m\right]^{-1} + \frac{V_i}{V_i + V_p}\left[S_p + (C_i - C_m)^{-1}C_m\right]^{-1}\right\} \qquad (2.11)$$

In the same way as for the general two-phase Mori-Tanaka model above, m indicates the matrix phase and p the inclusion phase, whereas i now indicates the interphase. Furthermore, V_m is the volume fraction of the matrix, V_p is the volume fraction of the inclusions, and V_i is the volume fraction of the interphase. Moreover, C_m is the stiffness matrix of the matrix, C_p is the stiffness matrix of the inclusions, and C_i is the stiffness matrix of the inclusions. Finally, I is the identity matrix and S_p is the Eshelby tensor of the particles, which in the model by Odegard *et al.* is said to be spherical. The Eshelby tensor may, however, easily be varied for different spheroidal shapes.

2.3 An effective interphase model for randomly oriented inclusions

The effective interphase model described in Section 2.2 only takes spherical particles into account. As a consequence of this, the particles can be considered as aligned. An extension of the model to also include randomly oriented inclusions with an interphase, and with spheroidal shapes different from spheres (i.e. prolate and oblate shape), will be presented here. The idea is that the same "averaging strategy", as was applied for the general multi-phase Mori-Tanaka model for randomly oriented inclusions described in Section 2.1, can be applied for the interphase model.

By comparing the terms in the general multi-phase Mori-Tanaka model and the effective interphase model, we find the terms that need to be orientationally averaged. The composite stiffness for such a composite can then be expressed as,

$$C_C = C_m + \left[\left(V_p + V_i\right)\left\{\left(C_i - C_m\right) A_{pi}\right\} + V_p \left\{\left(C_p - C_i\right) A_p\right\} \right] \left[V_m I + \left(V_p + V_i\right) A_{pi} \right]^{-1} \qquad (2.12)$$

where the curly brackets indicate the average of the quantity over all possible orientations. To the author's knowledge, this model has not been published elsewhere.

In the same way as reported for the general multi-phase Mori-Tanaka model for randomly oriented inclusions [1], the latter factor in the above expression, i.e. A_{pi}, is not averaged in case of spherical inclusions, but averaged for prolate and oblate spheroidal inclusions. As reported in [1], there is presently no full understanding of why this is required.

3 Interphase volume fraction

When considering a nanocomposite with an interphase region in addition to the particles and the neat polymer matrix, a re-calculation of the volume fractions of the composite must be performed. Instead of the two phases (matrix and particles), the total volume of the composite is now a sum of three volume fractions, that is

$$1 = V_p + V_i + V_m \qquad (3.1)$$

where, as in the expressions in the previous section, V_p is the volume fraction of the particles, V_i is the volume fraction of the interphase, and V_m is the volume fraction of the neat matrix.

The volume fraction of the interphase can be calculated from the volume of the composite.

3.1 Spherical inclusions

When assuming spherical shaped inclusions, the volume of the particle v_p and the interphase region v_i can be calculated from the general expression for the volume of a sphere: $v = 4/3\,\pi r^3$. Assuming now that the radius of the particle is r_p, and that the interphase region has a radius that is n times the radius of the particle, the volume of the interphase can be calculated as

$$v_i = \frac{4}{3}\pi(nr_p)^3 - \frac{4}{3}\pi r_p^3 = \frac{4}{3}\pi r_p^3 (n^3 - 1) = (n^3 - 1)v_p \qquad (3.2)$$

Hence, the volume of the interphase is $(n^3 - 1)$ times the volume of the particle. From this follows that the volume fraction of the interphase is $(n^3 - 1)$ times the volume fraction of the particles.

Employing (3.2), the volume fraction of the different constituent materials of the nanocomposite may then be expressed as

$$V_i = (n^3 - 1)V_p$$
$$V_m = 1 - (n^3 - 1)V_p - V_p = 1 - n^3 V_p \tag{3.3}$$

The parameter n will in the rest of this report be referred to as the *interphase thickness factor*.

3.2 Spheroidal shaped inclusions

In the same way as for the special case of spherical inclusions (where $a = b = c$), the volume fraction of the interphase can be calculated for the other spheroidal shaped particles (i.e. oblate and prolate). Assuming that the half axis for the interphase region is n times the half axis of the particle, we end up with the same expressions as in (3.3). This should be quite accurate for most particles, maybe except for inclusions where $c \gg a = b$.

3.3 Fibre-like inclusions

Fisher and Brinson [3] present a formula for calculating the interphase volume fraction for CNTs and other fibre-like particles. The expression is based on simple calculations of the volume of cylinders,

$$V_i = \left(\left(\frac{t}{r_p} \right)^3 + 2\left(\frac{t}{r_p} \right) \right) V_p \tag{3.4}$$

In the above expression, t denotes the thickness of the interphase region, whereas the rest of the parameters are defined earlier. Assuming, in the same way as in Section 3.1 and Section 3.2, that the interphase is n times the particle radius, we end up with the same expression for the volume fraction of the interphase as in (3.3).

4 Composite material systems

Two different composite material systems will be applied for comparison of the model results in Section 5. The same material systems will be used in the comparison between model results and experimental data in Section 6.

The material data for a nanoalumina/epoxy composite are taken from Johnsen *et al.* [12], and given in Table 4.1. The table also includes the elastic properties which are assumed and applied for the interphase.

Table 4.1 Material data for nanoalumina/epoxy composites [12].

Material parameter	Unit	Value	Comment
Matrix:			
Young's modulus	GPa	3.12	
Poisson's ratio		0.35	
Alumina inclusion:			
Young's modulus	GPa	386	
Poisson's ratio		0.22	
Interphase:			
Young's modulus	GPa	1.0-4.0	Varied
Poisson's ratio		0.35	

The material properties for a nanosilica/epoxy composite are taken from Johnsen *et al.* [13], and given in Table 4.2. In a similar way as for the first material system, the table also includes the elastic properties which are assumed and applied for the interphase.

Table 4.2 Material properties for a nanosilica/epoxy composite.[13].

Material parameter	Unit	Value	Comment
Matrix:			
Young's modulus	GPa	2.96	
Poisson's ratio		0.35	
Silica inclusion:			
Young's modulus	GPa	70	
Poisson's ratio		0.20	
Interphase:			
Young's modulus	GPa	1.0-4.0	Varied
Poisson's ratio		0.35	

5 Comparison of model results

For comparison of model results, that is, comparing the general multi-phase Mori-Tanaka model with the Odegard *et al.* interphase model, we use the material data for the nanosilica/epoxy composite [13].

5.1 Spherical inclusions

The interphase model, see Section 2.2, is established for composites with spherical particles. Our first test case is therefore analysis of this type of composites. Two model parameters are varied: 1) The elastic stiffness of the interphase, and 2) the interphase thickness factor.

First, the elastic stiffness of the interphase is set to $E_i = 1.0$ GPa, which is much lower than the elastic stiffness of the neat polymer, whereas the interphase thickness factor is varied. As can be

observed in Figure 5.1, the composite stiffness is reduced when increasing the interphase thickness factor. For a certain interphase thickness value, the composite elastic stiffness becomes lower than the neat polymer stiffness for all volume fractions. This is as expected, and can be explained by the volume fraction of the interphase. When the volume fraction of the interphase region becomes large, a larger volume fraction (of the matrix) has a lower stiffness than the neat matrix, resulting in reduced composite stiffness. For a given value of n, the entire matrix area is contained in the interphase region, and the composite stiffness is reduced below the bulk matrix stiffness – even for low particle concentrations.

Since the interphase thickness factor is higher than 1.0 for all the displayed curves, the two-phase Mori-Tanaka model predicts a higher elastic stiffness than the interphase model. This is also as expected. Note that the composite stiffness obtained from the Mori-Tanaka model is equal to the stiffness obtained by setting $n = 1.0$ in the interphase model; the latter curve is not shown in this case.

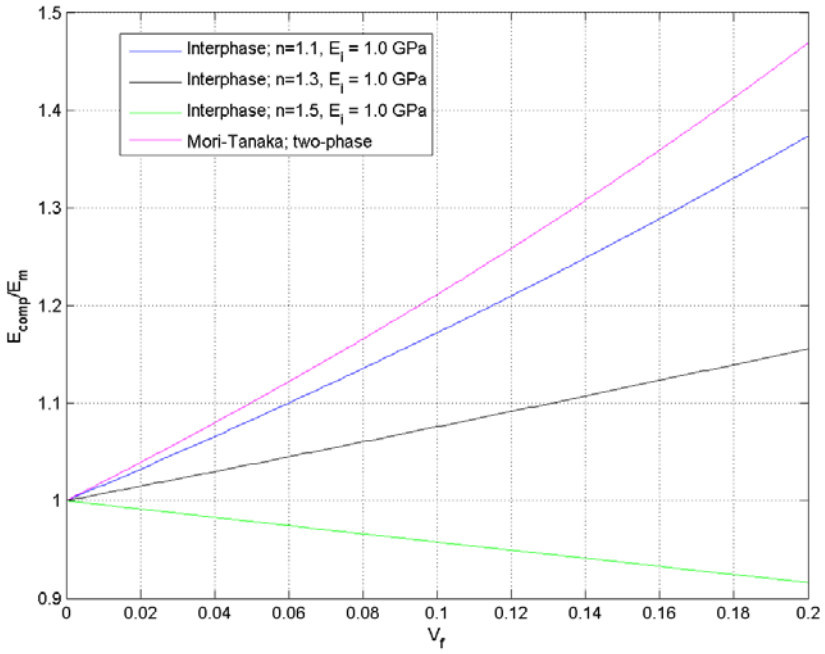

Figure 5.1 Composite elastic stiffness for a composite with spherical inclusions. The interphase elastic stiffness is set to 1.0 GPa, whereas the interphase thickness factor is varied.

Second, the elastic stiffness of the interphase is set to $E_i = 4.0$ GPa, which is higher than the elastic stiffness of the neat matrix, whereas the interphase thickness factor is varied. As shown in Figure 5.2, the composite stiffness is increased when increasing the interphase thickness factor. This is as expected. Following a similar argumentation as in the first case, when the volume fraction of the interphase region becomes larger, a larger volume fraction of the matrix has a higher stiffness than the neat matrix, resulting in a higher composite elastic stiffness.

The two-phase Mori-Tanaka model predicts a lower elastic stiffness than the interphase model for all volume fractions. This is also as expected, because a composite with an interphase region with

a higher elastic stiffness will give a higher composite elastic stiffness compared to the case of no interphase region. Again, the composite stiffness obtained from the Mori-Tanaka model is equal to the stiffness obtained by setting $n = 1.0$ in the interphase model.

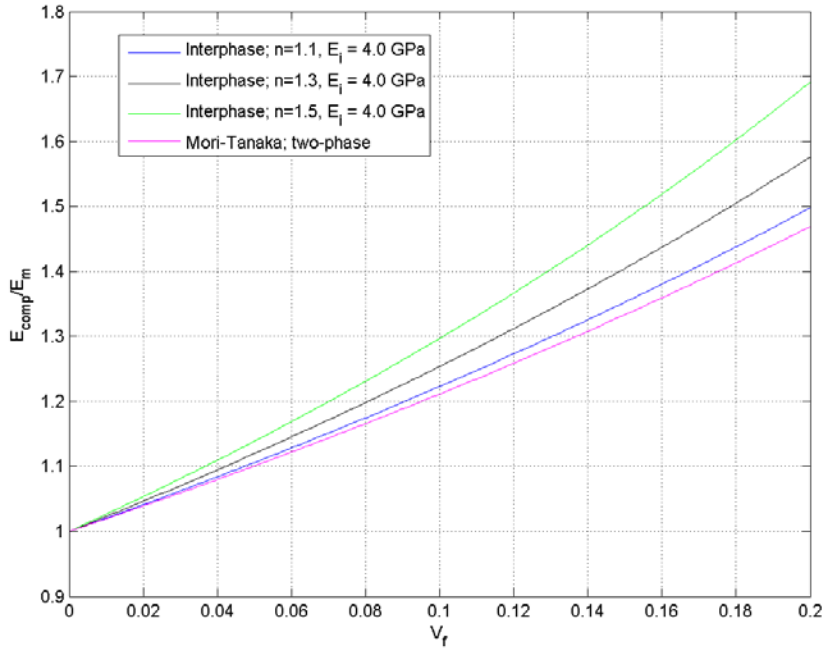

Figure 5.2 Composite elastic stiffness for a composite with spherical inclusions. The interphase elastic stiffness is set to 4.0 GPa, whereas the interphase thickness factor is varied.

5.2 Aligned prolate spheroidal inclusions

To compare the two-phase Mori-Tanaka model and the interphase model for aligned particles, test cases are run for prolate (i.e. elongated) spheroidal shaped inclusions. As mentioned above, the Odegard *et al.* model only included spherical inclusions. Thus, this may be seen as an extension of their model, as well as a verification of the implemented code for other spheroidal shapes.

In the same way as in Section 5.1, the interphase elastic stiffness and the interphase thickness factor is varied. For all cases the aspect ratio of the inclusions is set to $\alpha = 3$.

First, the elastic stiffness of the interphase is set to $E_i = 1.0$ GPa, which is much lower than the elastic stiffness of the neat matrix, whereas the interphase thickness factor is varied. As can be observed in Figure 5.3, the composite stiffness is reduced for an increasing value of n. This is as expected. As for the case of spherical particles, a larger volume fraction of the matrix gets a lower stiffness than the bulk matrix when the interphase region is increased, and the composite stiffness is reduced.

The Mori-Tanaka model predicts higher stiffness than the interphase model; the same curve is obtained by setting $n = 1.0$ in the interphase model. These results are also as expected.

Comparing the composite elastic stiffness obtained for the composite with prolate spheroidal inclusions with the corresponding composite with spherical inclusions (i.e. the first case in Section 5.1), we observe that the composite with prolate spheroidal inclusions have a higher elastic stiffness.

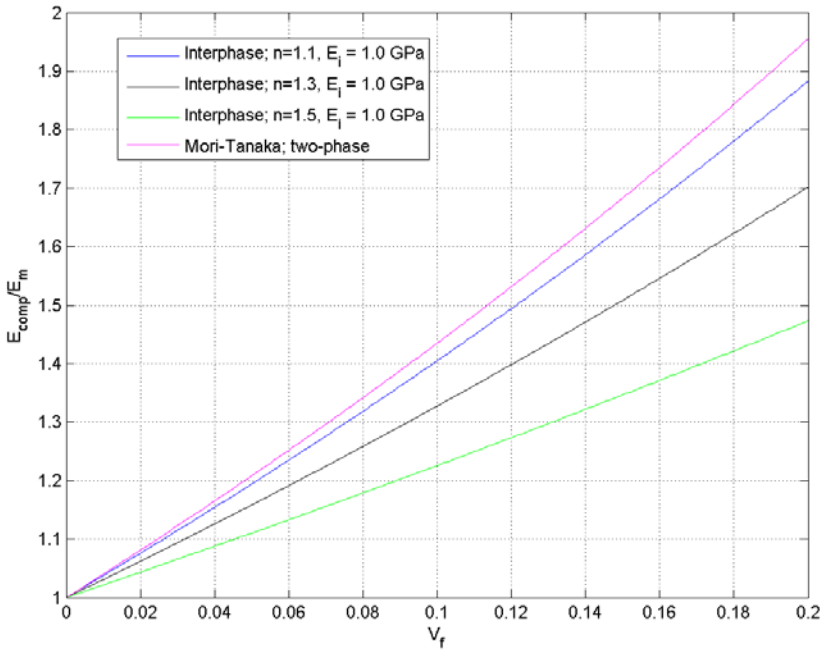

Figure 5.3 Composite elastic stiffness for a composite with aligned prolate spheroidal inclusions. The interphase elastic stiffness is set to 1.0 GPa, whereas the interphase thickness factor is varied.

Second, the elastic stiffness of the interphase is set to $E_i = 4.0$ GPa, which is higher than the matrix bulk elastic stiffness, whereas the interphase thickness factor is varied. As is displayed in Figure 5.4, the composite stiffness is increased for increasing values of n. The same argumentation as in the previous cases applies: When the volume fraction of the interphase region becomes larger, a larger volume fraction of the matrix has a higher stiffness than the neat matrix, resulting in a higher composite elastic stiffness. This is as expected. Moreover, the Mori-Tanaka model predicts lower stiffness than the interphase model for all values.

Comparing the composite elastic stiffness of the composite with prolate shaped inclusions with the corresponding composite with spherical particles (i.e. second case in Section 5.1), we observe that the composite with prolate spheroidal inclusions have a higher elastic stiffness.

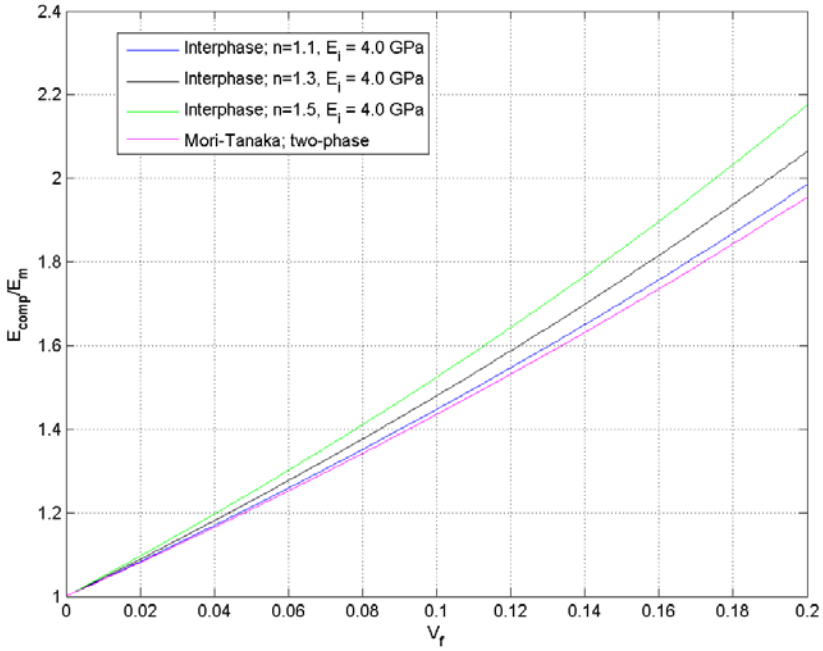

Figure 5.4 Composite elastic stiffness for a composite with aligned prolate spheroidal inclusions. The interphase elastic stiffness is set to 4.0 GPa, whereas the interphase thickness factor is varied.

5.3 Aligned oblate spheroidal inclusions

Composites with aligned oblate (i.e. contracted) spheroidal inclusions are also considered. The calculated elastic stiffness for the two-phase Mori-Tanaka model and the interphase model is compared. As for the prolate inclusion case, this may be seen as an extension of the Odegard *et al.* model, as well as a verification of the implemented code for other spheroidal shaped inclusions different from spherical.

The interphase elastic stiffness and the interphase thickness factor are varied. The aspect ratio of the inclusions is in this case set to $\alpha = 1/3$.

First, the elastic stiffness of the interphase is set to $E_i = 1.0$ GPa, which is much lower than the matrix bulk elastic stiffness, whereas the interphase thickness factor is varied.

As shown in Figure 5.5 , the elastic stiffness of the composite is reduced for increasing values of n. For a certain interphase thickness value, the composite elastic stiffness becomes lower than the neat polymer stiffness for all volume fractions. This is as expected, and can again be explained by the volume fraction of the interphase. Also, for a given value of n, the entire matrix area is included in the interphase region, and the composite stiffness is reduced below the bulk matrix stiffness – even for low particle concentrations.

The Mori-Tanaka model predicts a higher stiffness than the interphase model for all values; the same stiffness curve is obtained by setting $n = 1.0$ for the interphase model.

When comparing the composite elastic stiffness of the composite to oblate shaped inclusions with the corresponding composite with spherical particles (i.e. first case in Section 5.1), we observe that the composite with oblate spheroidal inclusions have a lower elastic stiffness, which is as expected.

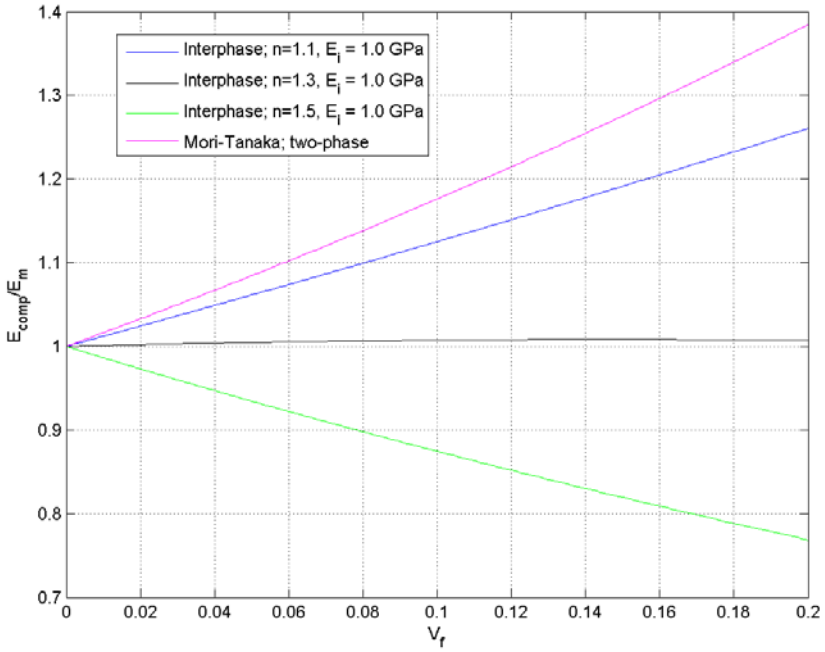

Figure 5.5 Composite elastic stiffness for a composite with aligned oblate spheroidal inclusions. The interphase elastic stiffness is set to 1.0 GPa, whereas the interphase thickness factor is varied.

Second, the elastic stiffness of the interphase is set to $E_i = 4.0$ GPa, which is higher than the elastic stiffness of the neat matrix, whereas the interphase thickness factor is varied. As is observed in Figure 5.6, the composite elastic stiffness is increased for increasing values of n. The same argumentation as in the previous cases applies: When the volume fraction of the interphase region becomes larger, a larger volume fraction of the matrix has a higher stiffness than the neat matrix, resulting in a higher composite elastic stiffness. This is as expected. Moreover, the Mori-Tanaka model predicts lower stiffness than the interphase model for all values; the same stiffness is obtained by setting $n = 1.0$ in the interphase model.

When comparing the composite elastic stiffness of the composite with oblate shaped inclusions with the corresponding composite with spherical particles (i.e. second case in Section 5.1), we observe that the composite with oblate spheroidal inclusions have a lower elastic stiffness. This is as expected.

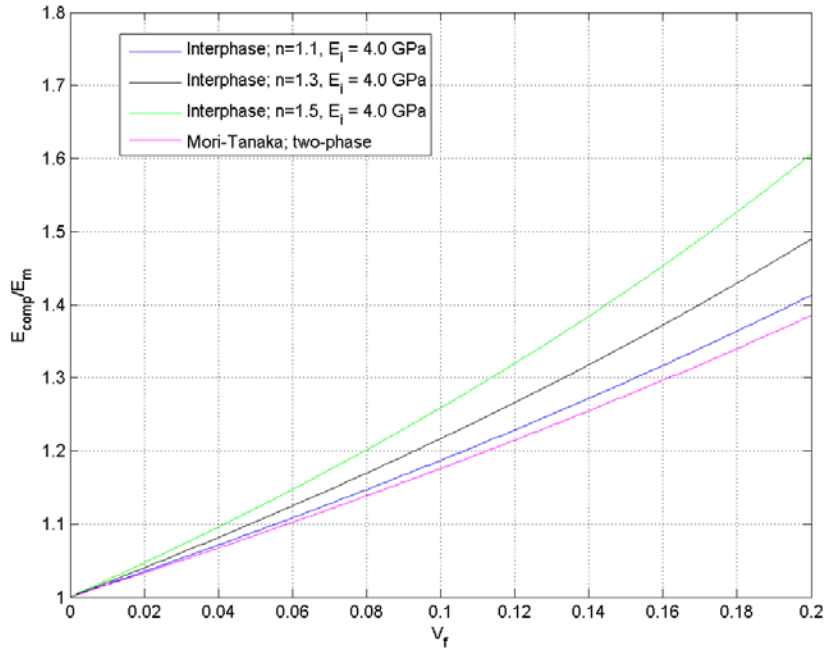

Figure 5.6 Composite elastic stiffness for a composite with aligned oblate spheroidal inclusions. The interphase elastic stiffness is set to 4.0 GPa, whereas the interphase thickness factor is varied.

5.4 Randomly oriented prolate spheroidal inclusions

In this next test case, the composite elastic stiffness calculated for the two-phase Mori-Tanaka model and the interphase model is compared for a composite with randomly oriented prolate spheroidal inclusions. This case is an extension of the model presented by Odegard *et al.* [11], where the model expressions for the interphase model are presented in Section 2.3.

As for the previous cases, the interphase elastic stiffness and the interphase thickness factor is varied. The aspect ratio of the inclusions is set to $\alpha = 3$, which is the same value as employed for the corresponding composite with aligned inclusions described in Section 5.2.

First, the elastic stiffness of the interphase is set to $E_i = 1.0$ GPa, which is much lower than the elastic stiffness of the neat matrix, whereas the interphase thickness factor is varied. As shown in Figure 5.7, the elastic stiffness of the composite stiffness is decreasing for increasing values of n. For a certain interphase thickness value, the composite elastic stiffness becomes lower than the neat polymer stiffness for all volume fractions. This is as expected, and can be explained by the increasing volume fraction of the interphase. For a given value of n, the entire matrix area is included in the interphase region, and the composite stiffness is reduced below the bulk matrix stiffness – even for low particle concentrations.

The Mori-Tanaka model predicts higher stiffness than the interphase model for all values, except for the case where $n = 1.0$. In this case the elastic stiffness calculated by the two models is very similar for volume fractions up to 0.2; the deviation is believed to be round-off errors in the

calculations. This indicates that the averaging strategy proposed for the interphase model is applicable.

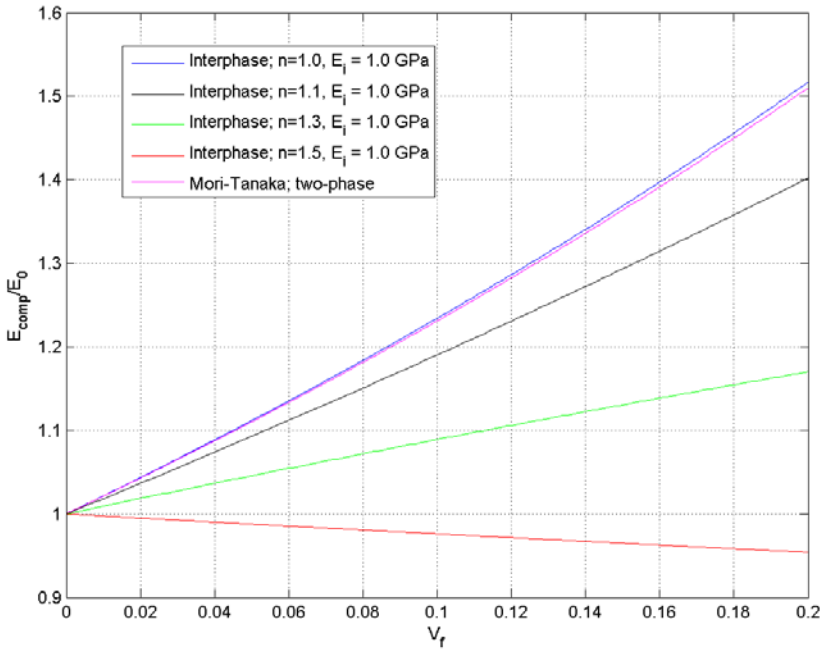

Figure 5.7 Composite elastic stiffness for a composite with randomly oriented prolate spheroidal inclusions. The interphase elastic stiffness is set to 1.0 GPa, whereas the interphase thickness factor is varied.

Second, the elastic stiffness of the interphase is set to $E_i = 4.0$ GPa, which is higher than the elastic stiffness of the neat matrix, whereas the interphase thickness factor is varied. As shown in Figure 5.8, the elastic stiffness of the composite is increased for increasing values of n. The same argumentation as in the previous cases applies: When the volume fraction of the interphase region becomes larger, a larger volume fraction of the matrix has a higher stiffness than the neat matrix, resulting in a higher composite elastic stiffness. This is as expected.

The Mori-Tanaka model predicts lower stiffness than the interphase model. For the case of $n = 1.0$ in the interphase model, the elastic stiffness calculated by the two models is close to the same for volume fractions up to 0.2; the deviation is believed to be round-off errors in the calculations. Again, this indicated that the averaging strategy proposed for the interphase model is applicable.

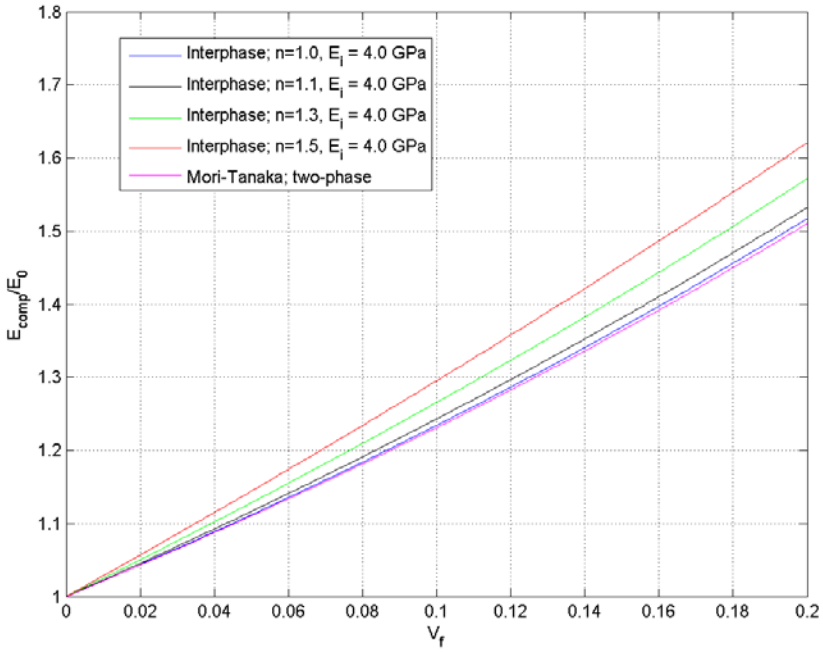

Figure 5.8 Composite elastic stiffness for a composite with randomly oriented prolate spheroidal inclusions. The interphase elastic stiffness is set to 4.0 GPa, whereas the interphase thickness factor is varied.

5.5 Random oriented oblate spheroidal inclusions

The composite elastic stiffness calculated for the two-phase Mori-Tanaka model and the interphase model is next compared for a composite with randomly oriented oblate spheroidal inclusions. This case is an extension of the model presented by Odegard *et al.* [11], where the model expressions for the interphase model are presented in Section 2.3.

As for the previous cases, the interphase elastic stiffness and the interphase thickness factor is varied. The aspect ratio of the inclusions is set to $\alpha = 1/3$, which is the same value as employed for the corresponding composite with aligned oblate inclusions described in Section 5.2. With this aspect ratio, the elastic stiffness for the composite with random oriented oblate spheroidal shaped inclusions should be equal to the elastic stiffness of the composite with random oriented prolate spheroidal inclusions, see Section 5.4 (where the aspect ratio was set to $\alpha = 3$).

First, the elastic stiffness of the interphase is set to $E_i = 1.0$ GPa, which is much lower than the elastic stiffness of the neat matrix, whereas the interphase thickness factor is varied. As displayed in Figure 5.9, the elastic stiffness of the composite is decreasing for increasing values of n. For a certain interphase thickness value, the composite elastic stiffness becomes lower than the neat polymer stiffness for all volume fractions. This is as expected, and can be explained by the increasing volume fraction of the interphase. For a given value of n, the entire matrix area is included in the interphase region, and the composite stiffness is reduced below the bulk matrix stiffness – even for low particle concentrations.

The Mori-Tanaka model predicts higher stiffness than the interphase model for all values, except for the case where $n = 1.0$. In this case the elastic stiffness calculated by the two models is close to the same for volume fractions up to 0.2, which also in this case indicates that the averaging strategy proposed for the interphase model is applicable.

When comparing the calculated elastic stiffness for the composite with randomly oriented oblate spheroidal inclusions to the corresponding calculated stiffness for the composite with randomly oriented prolate spheroidal inclusions (see first case in Section 5.4), the results agree well. This is as expected.

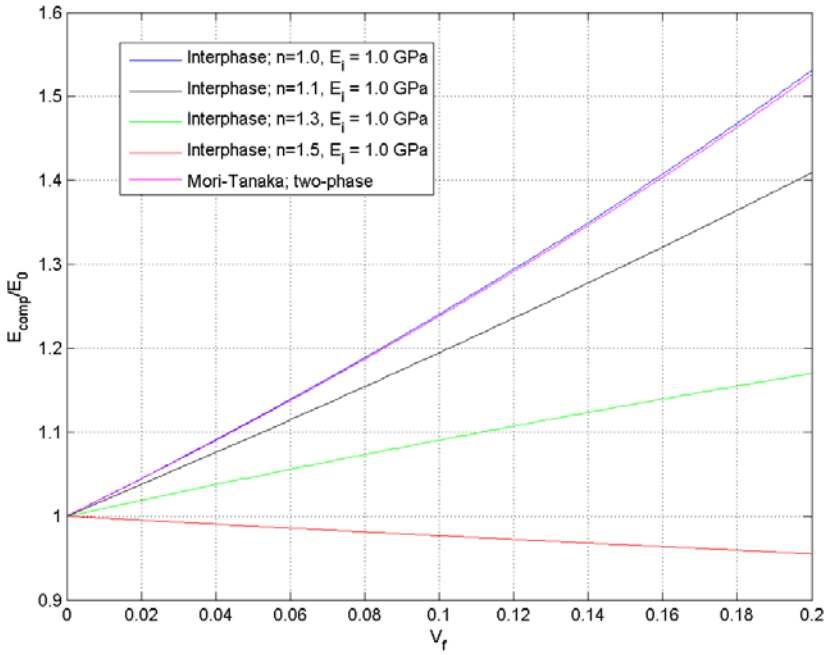

Figure 5.9 Composite elastic stiffness for a composite with randomly oriented oblate spheroidal inclusions. The interphase elastic stiffness is set to 1.0 GPa, whereas the interphase thickness factor is varied.

Second, the elastic stiffness of the interphase is set to $E_i = 4.0$ GPa, which is higher than the elastic stiffness of the neat matrix, whereas the interphase thickness factor is varied. As shown in Figure 5.10, the elastic stiffness of the composite is increased for increasing values of n. The same argumentation as in the previous cases applies: When the volume fraction of the interphase region becomes larger, a larger volume fraction of the matrix has a higher stiffness than the neat matrix, resulting in a higher composite elastic stiffness. This is as expected.

The Mori-Tanaka model predicts lower stiffness than the interphase model. For the case of $n = 1.0$ in the interphase model, the elastic stiffness calculated by the two models is close to the same for volume fractions up to 0.2, which indicated that the averaging strategy proposed for the interphase model is applicable.

When comparing the calculated elastic stiffness for the composite with randomly oriented oblate spheroidal inclusions to the corresponding calculated stiffness for the composite with randomly oriented prolate spheroidal inclusions (see second case in Section 5.4), the results agree well. This is as expected.

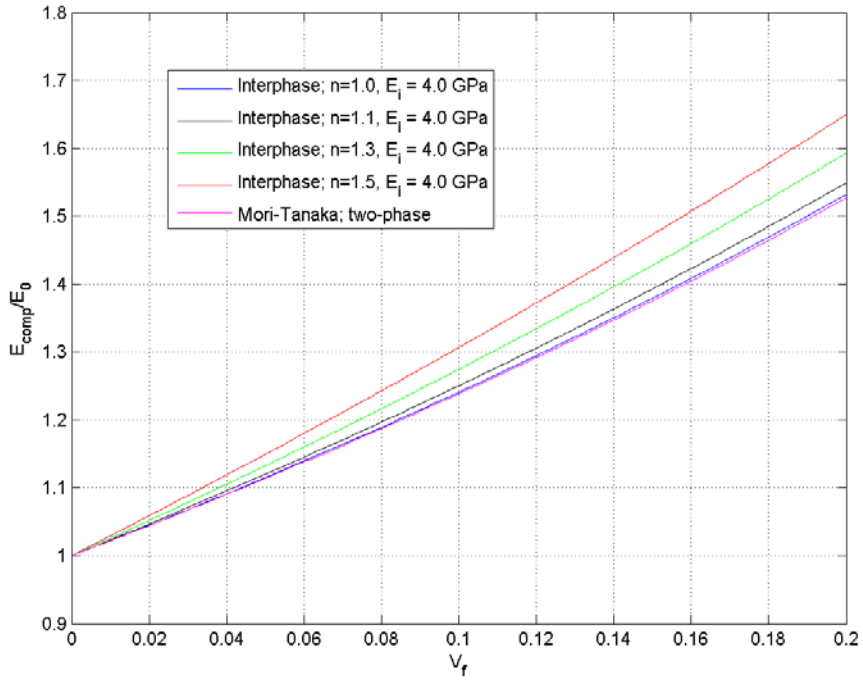

Figure 5.10 Composite elastic stiffness for a composite with randomly oriented oblate spheroidal inclusions. The interphase elastic stiffness is set to 4.0 GPa, whereas the interphase thickness factor is varied.

5.6 Two special cases

Two special cases where the interphase model seems to calculate an unphysical stiffness should be noted. This is demonstrated for the composite with spherical inclusions, but this also yields for other spheroidal inclusions.

5.6.1 Case 1: Zero stiffness at the interphase

The general two-phase Mori-Tanaka model has been reported by Thorvaldsen [1] to work for composites with voids, i.e. an inclusion phase with zero stiffness. The elastic stiffness of the "composite" is then reduced, compared to the neat matrix stiffness. For the interphase model, a similar result should be obtained in the case where the interphase region has zero stiffness. In such a situation, the particles will not contribute to the composite stiffness, but still be part of the volume of the composite, i.e. a volume fraction higher than zero.

Figure 5.11 displays the calculated elastic stiffness employing the interphase model for a composite with interphase elastic stiffness equal to zero. As can be observed in the figure, the interphase model calculates a stiffness increase in case of an interphase thickness factor value close to 1.0. For higher values of the interphase thickness factor, the elastic stiffness of the

composite is reduced. An interphase thickness factor of $n = 1.45$ in the interphase model, gives a composite stiffness which is close to the stiffness obtained from the two-phase Mori-Tanaka model.

The interphase model generally calculates a composite stiffness that is unphysical and not according to other model calculations and experimental data. The interphase model should thus not be applied in this case, as it requires non-zero interphase stiffness.

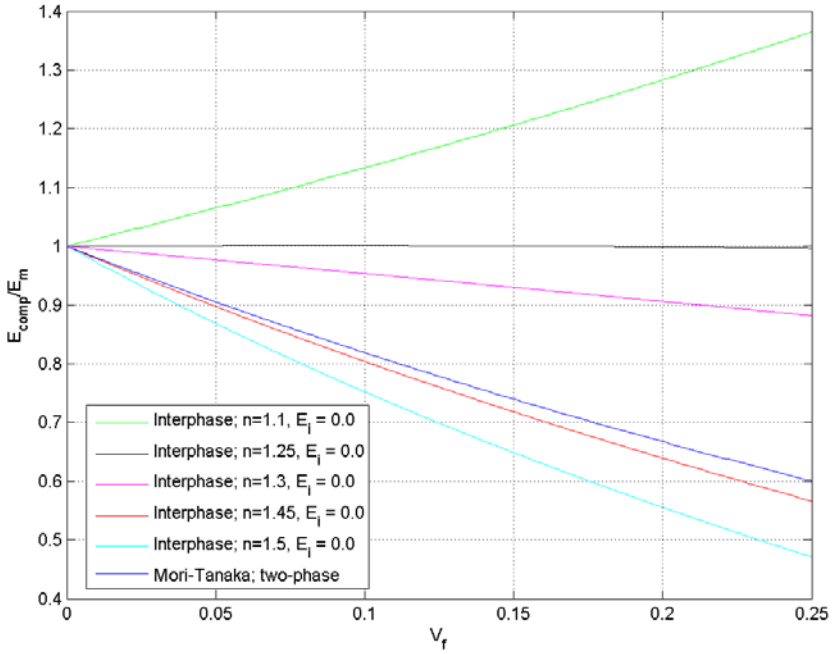

Figure 5.11 Elastic stiffness for a composite with voids. For the interphase model the interphase elastic stiffness is set to zero.

5.6.2 Case 2: Interphase elastic stiffness equal to the neat matrix stiffness

In the case where the interphase elastic stiffness is equal to the stiffness of the bulk matrix, no interphase is actually present in the composite. The calculated stiffness employing the interphase model should then be equal to the composite elastic stiffness obtained from the two-phase Mori-Tanaka model.

From considering the stiffness expression for the interphase model in (2.11) , we easily see that we end up with inverting a zero matrix in case $C_i = C_m$. The zero matrix is singular, and cannot be inverted. Hence, the interphase model is not applicable for this special case.

6 Comparison with experimental results

The purpose of this section is to make an initial and brief comparison between the calculated elastic stiffness and experimental data for some relevant nanocomposites. A more detailed and thorough analysis is found in [7]. For the two composite systems given in Section 4, stiffness data from experimental tests is available.

6.1 Alumina/epoxy composite

6.1.1 Spherical inclusions

Experimental data for spherical nanoalumina particles embedded in epoxy is given in Table 6.1. Two different techniques are applied for the dispersion of the particles, that is, horn sonication and bath sonication. Moreover, a silane (GPS) surface treatment is applied for improving the adhesion between the particles and the surrounding matrix. More details are found in [12]. The data set is very small, which means that it may be difficult to draw any conclusions on the agreement between the calculated elastic stiffness and the experimental values. However, improved understanding on the effect of alumina inclusions can be obtained.

Table 6.1 Experimental results for the elastic properties of epoxy/alumina nanocomposites with spherical inclusions. The data are taken from [12].

Material type	**Sonication**	**wt%**	**Nominal V_f**	**Tensile modulus, E (MPa)**
Epoxy	N/A	N/A	0.0	3.12 ± 0.11
NT-50nm	Bath	1.0	0.00350	3.15 ± 0.10
NT-50nm	Bath	4.0	0.01385	3.22 ± 0.13
NT-50nm	Horn	1.0	0.00345	3.40 ± 0.19
NT-50nm	Horn	2.9	0.01025	3.24 ± 0.070
GPS-50nm	Bath	3.0	0.01060	3.29 ± 0.13
GPS-50nm	Horn	1.0	0.00345	3.13 ± 0.06

(NT= Not treated; GPS = silane treated)

The magenta curve in Figure 6.1 gives the calculated elastic stiffness of the nanoalumina/epoxy composite with spherical inclusions, as a function of particle volume fraction, using the two-phase Mori-Tanaka model. The other curves display the calculated composite elastic stiffness employing the interphase model, with interphase elastic stiffness of 4.0 GPa and varying value of the interphase thickness factor.

As can be observed in the figure, there is good agreement between the model results and the experimental data in case of employing the bath sonication procedure for the untreated particles. In this case, the interphase thickness seems to be small, and do not significantly affect the composite stiffness. For the test specimen where the horn sonication procedure has been used, as well as the case of using bath sonication together with particle surface treatment, the interphase model with a higher interphase thickness factor value seems to better estimate the composite elastic stiffness. One explanation for the composite stiffness increase is that the GPS surface treatment actually improves the interphase properties. The reason for the stiffness improvement for the untreated particle case is more difficult to explain. For the specimens where the GPS treated particles are dispersed using the horn sonication, the models overestimate the elastic stiffness of the composite.

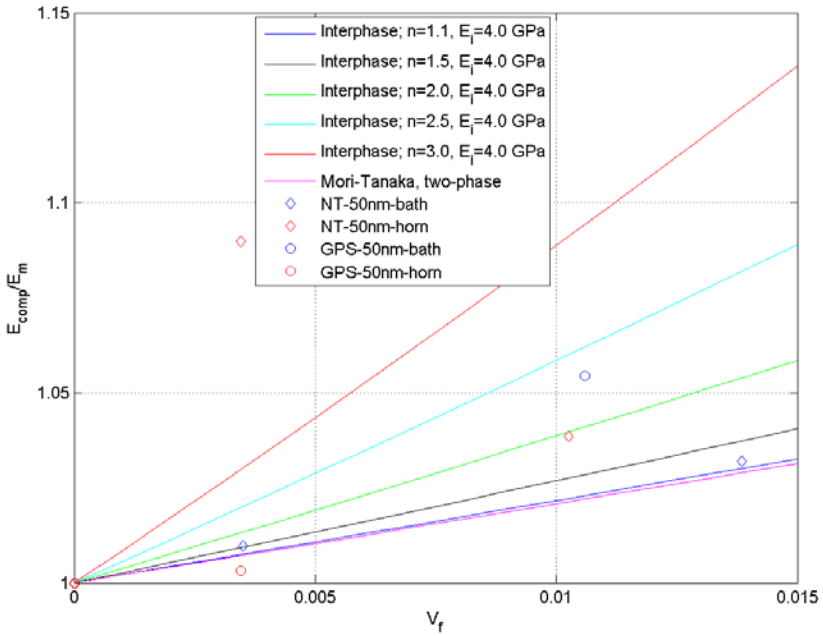

Figure 6.1 Alumina/epoxy nanocomposite. Experimental data is taken from Johnsen et al. [12].

6.1.2 Fibre-like inclusions

The experimental data for alumina whisker inclusions are shown in Table 6.2. In the same way as for the spherical particles, two different sonication techniques are applied. In this case, no surface treatment is applied for improving the adhesion between the particles and the surrounding matrix. In the same way as in [1], the aspect ratio is set to 20, which is chosen to get a best fit with the experimental data for the composite elastic stiffness calculated by the two-phase Mori-Tanaka model. In the same way as for the spherical alumina particles, more data is required before drawing any conclusions on the behaviour and properties of the nanocomposite.

Table 6.2 Experimental results for the elastic properties of epoxy/alumina nanocomposites with fibre-like inclusions. The data are taken from [12].

Material type	**Sonication**	**wt%**	**Nominal V_f**	**Tensile modulus, E**
Epoxy	N/A	N/A	0.0	3120 ± 110
NT-wiskers	Bath	0.1	0.00035	3310 ± 140
NT-wiskers	Bath	1.0	0.00350	3360 ± 110
NT-wiskers	Bath	3.0	0.01060	3450 ± 170
NT-wiskers	Bath	5.0	0.01730	3540 ± 130
NT-wiskers	Horn	0.1	0.00035	3210 ± 190
NT-wiskers	Horn	1.0	0.00345	3390 ± 120
NT-wiskers	Horn	2.9	0.01025	3360 ± 140

(NT= Not treated)

The calculated elastic stiffness is shown together with the experimental data in Figure 6.2. The calculated composite stiffness using the interphase model agrees very well with the stiffness

obtained from the two-phase Mori-Tanaka model in case of no interphase (i.e. $n = 1.0$). For a composite with an interphase elastic stiffness higher than the neat matrix and an interphase thickness factor higher than 1.0, the calculated composite stiffness is increased compared to the bulk matrix. On the other hand, for a composite with an interphase elastic stiffness lower than the neat matrix and an interphase thickness factor higher than 1.0, the calculated composite stiffness is decreased compared to the neat matrix.

As can also be observed in the figure, the model composite with improved properties for the interphase estimates a stiffness which is closer to the stiffness values obtained experimentally, but the interphase model is not able to estimate the significant stiffness improvements for very low particle volume fractions. Thus, the reason for this significant stiffness increase seems not to be due to interphase effects.

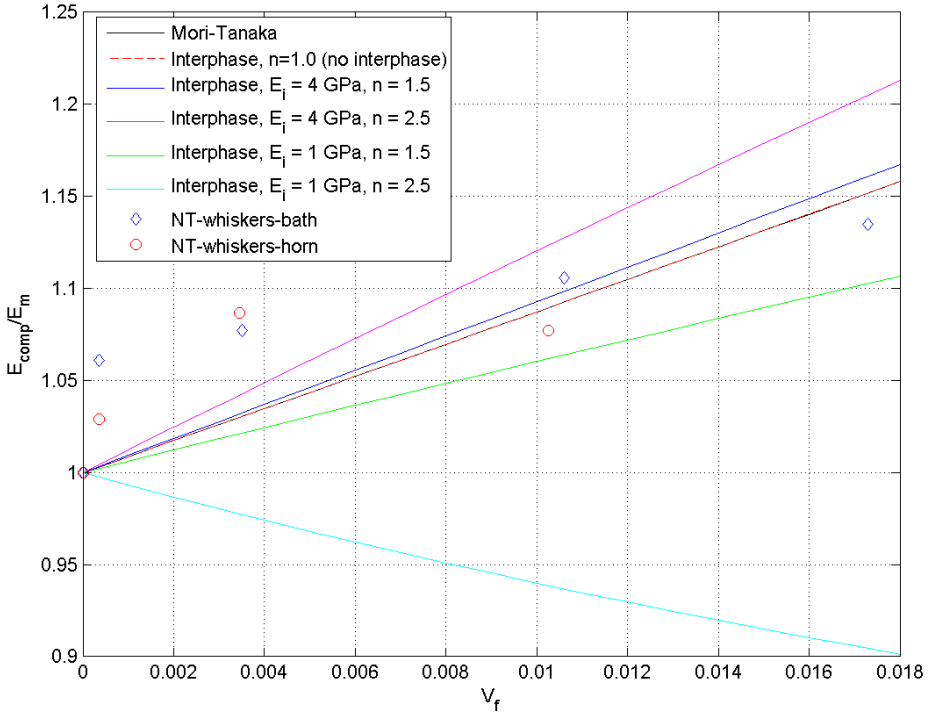

Figure 6.2 Composite with randomly oriented alumina whiskers. The experimental data are taken from Johnsen et al. [12].

6.2 Nanosilica-epoxy composite with spherical particles

Experimental results for the elastic stiffness of silica/epoxy nanocomposites are reported by Johnsen *et al.* [13]. The obtained elastic stiffness values for the nanocomposites with spherical nanosilica particles are given in Table 6.3.

Table 6.3 Experimental results for the elastic properties of silica/epoxy composites with spherical inclusions. The data are taken from[13].

Material type	**wt%**	**Nominal V_f**	**Tensile modulus, E (MPa)**
Epoxy	N/A	0.0	2960 ± 200
Nanosilica-epoxy	4.1	0.025	3200 ± 150
Nanosilica-epoxy	7.8	0.049	3420 ± 180
Nanosilica-epoxy	11.1	0.071	3570 ± 130
Nanosilica-epoxy	14.8	0.096	3600 ± 50
Nanosilica-epoxy	20.2	0.134	3850 ± 240

The calculated composite elastic stiffness together with the experimental data is displayed in Figure 6.3. As can be observed, the interphase thickness seems to vary as a function of particle volume fraction in this case. For high volume fractions, the interphase does not seem to significantly influence the composite elastic stiffness. The calculated results for both the two-phase Mori-Tanaka model and the interphase model with an interphase thickness close to 1.0 agree well with the experimental data. For low volume fractions, on the other hand, the stiffness increase may be due to improved elastic properties of the interphase.

Note, however, that the applied properties for the interphase may not be physically representative. This will, however, not be analysed further in this report. A more thorough discussion of the interphase stiffness properties and the interphase thickness factor is found in [7].

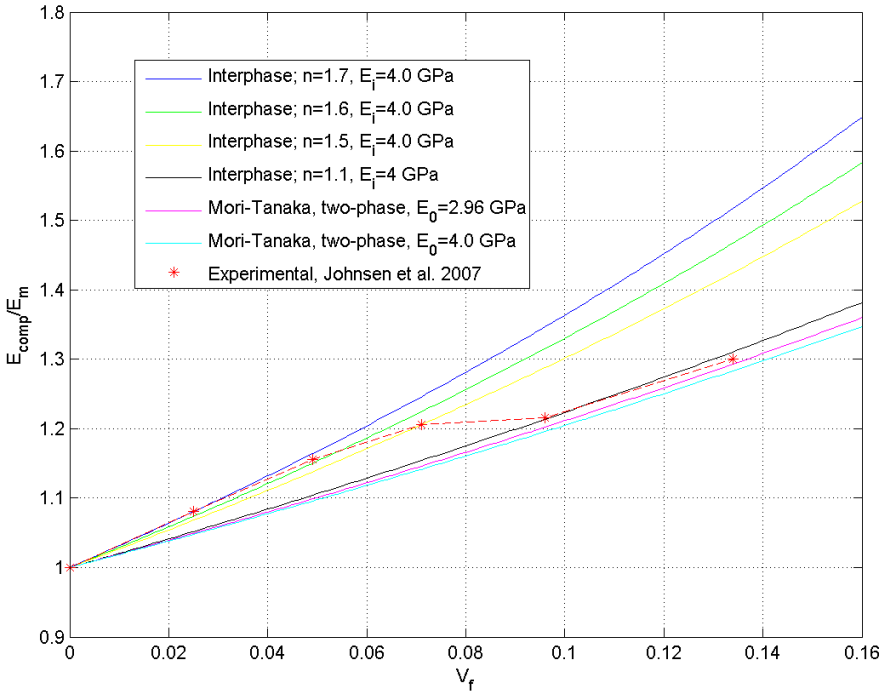

Figure 6.3 Silica/epoxy composite. The experimental results are taken from Johnsen et al. [13].

7 Summary

In this report, the interphase model by Odegard *et al.* [11] for calculation of the elastic stiffness of composites is described. The interphase is defined as the layer surrounding the particle. The interphase has different elastic properties compared to the neat matrix (and the particle), and thus can be applied for describing changes in the polymer structure due to the inclusions, the bonding properties between the particle and the matrix, as well as the increased composite elastic stiffness. Only spherical particles are considered and included in the interphase model. Extensions of the Odegard *et al.* interphase model that include non-spherical spheroidal inclusions are therefore presented. With the introduction of non-spherical inclusions, random orientation of the particles is also relevant. Expressions are thus presented for randomly oriented spheroidal inclusions. The general two-phase Mori-Tanaka, described and analysed in more detail in [1], is included for comparison.

The composite elastic stiffness calculated by the interphase model and the two-phase Mori-Tanaka model is found be agree well for different spheroidal inclusion shapes and orientations.

The composite stiffness calculations from using the interphase model are also compared with experimental data for two different nanocomposites. Based on a very brief and initial analysis, the model calculations are observed to agree with the experimental data. The significant stiffness increase may be explained by interphase effects. It seems, however, that the interphase thickness may be a function of the particle volume fraction. For high volume fractions an interphase thickness factor close to 1.0 makes the best fit with experimental data, meaning that the interphase does not significantly influence the composite stiffness. For low volume fractions a much higher interphase thickness value is required for the model calculations to agree with experimental data. In this latter case, the interphase effects are more significant.

A more thorough and detailed analysis of the use of the general Mori-Tanaka model and the interphase model, including a comparison with more experimental data, is found in [7]. Here, also a varying interphase thickness factor, as a function of particle volume fraction, is included in the models.

Future work should consider other factors that will influence the composite elastic stiffness, as well as other inclusion materials than those included in the current study. Graphene (or graphene oxide) is one relevant type of particle.

Acknowledgements

The author would like to thank Tyler P. Jones and Bernt B. Johnsen for reading the final version of this document and giving valuable comments and improvements to the text.

Appendix A Model summary

Table A.1 and Table A.2 give the Matlab file name for each of the implemented model, as well as reference to the paper and type of inclusion geometry.

The Matlab codes for all models are given in Appendix B.

Table A.1 Models for aligned inclusions.

File name	Reference	Inclusion geometry		
		Spherical	**Fibre-like**	**Disc shaped**
interphase_1.m	[11]	X	X	X
mori_tanaka_3.m	[3;14;15]	X	X	X

Table A.2: Models for randomly oriented inclusions.

File name	Reference	Inclusion geometry		
		Spherical	**Fibre-like**	**Disc shaped**
interphase_2.m	[11]	X	X	X
mori_tanaka_6.m	[3;14;15]	X	X	X

Appendix B Matlab code

B.1 General Mori-Tanaka model for aligned inclusions

```
% Mori-Tanaka – general model
% File name: “mori_tanaka_3.m”
% Generally: Model N-1 spheroidal shaped inclusions in an isotropic
matrix
% This case: One type of isotropic inclusion
% Three geometries:
% 1) aligned spherical inclusions
% 2) aligned fibre-like inclusions with aspect ratio
% 3) aligned disc-shaped inclusion with aspect ratio
%
% Author: Tom Thorvaldsen, FFI, March 2014

% Elastic properties - matrix
E_0 = 2.96
nu_0 = 0.35

C = zeros (6,6);
const = (E_0*(1-nu_0))/((1+nu_0)*(1-2*nu_0));
C(1,1) = const;
C(1,2)= const*(nu_0/(1-nu_0));
C(1,3)= const*(nu_0/(1-nu_0));
C(2,1) = C(1,2);
C(2,2) = const;
C(2,3) = const*(nu_0/(1-nu_0));
C(3,1) = C(1,3);
C(3,2) = C(2,3);
C(3,3) = const;
C(4,4) = const*((1-2*nu_0)/(2*(1-nu_0)));
C(5,5) = const*((1-2*nu_0)/(2*(1-nu_0)));
C(6,6) = const*((1-2*nu_0)/(2*(1-nu_0)));
C;

% Elastic properties - inclusion
E_i = 70
nu_i = 0.20

D = zeros (6,6);
const = (E_i*(1-nu_i))/((1+nu_i)*(1-2*nu_i));
D(1,1) = const;
D(1,2)= const*(nu_i/(1-nu_i));
```

```
D(1,3)= const*(nu_i/(1-nu_i));
D(2,1) = D(1,2);
D(2,2) = const;
D(2,3) = const*(nu_i/(1-nu_i));
D(3,1) = D(1,3);
D(3,2) = D(2,3);
D(3,3) = const;
D(4,4) = const*((1-2*nu_i)/(2*(1-nu_i)));
D(5,5) = const*((1-2*nu_i)/(2*(1-nu_i)));
D(6,6) = const*((1-2*nu_i)/(2*(1-nu_i)));
D;

% Geometry:
geom = 1  % spherical inclusions
%geom = 2  % fibre-like inclusions
%geom = 3  % disc shaped inclusions

if (geom == 1)
  % Spherical inclusions:
  S_1111 = (7-5*nu_0)/(15*(1-nu_0));
  S_2222 = S_1111
  S_3333 = S_1111
  S_1122 = (5*nu_0-1)/(15*(1-nu_0));
  S_1133 = S_1122
  S_2211 = S_1122
  S_2233 = S_1122
  S_3311 = S_1122
  S_3322 = S_1122
  S_1212 = (4-5*nu_0)/(15*(1-nu_0))
  S_1221 = S_1212
  S_2323 = S_1212
  S_2332 = S_1212
  S_3131 = S_1212
  S_3113 = S_1212

elseif (geom == 2)
  % Fiber-like inclusions:
  l = 1000       % fibre length
  d = 1       % fibre diameter
  a = l/d     % aspect ratio
  a2 = power(a,2.0)
  g = (a/power(a2-1,1.5))*(a*sqrt(a2-1)-acosh(a))
  b = 1/(1-nu_0)
```

```
  c = 1-2*nu_0
  e = 1/(a2-1)

  S_1111 = 0.5*b*(c + e*(3*a2-1)-(c+3*e*a2)*g)
  S_2222 = (3/8)*b*e*a2+0.25*b*(c-(9/4)*e)*g;
  S_3333 = S_2222;
  S_2233 = 0.25*b*(0.5*e*a2-(c+0.75*e)*g);
  S_3322 = S_2233;
  S_2211 = -0.5*b*e*a2 + 0.25*b*(3*e*a2-c)*g;
  S_3311 = S_2211;
  S_1122 = -0.5*b*(c+e)+0.5*b*(c+1.5*e)*g;
  S_1133 = S_1122;
  S_2323 = 0.25*b*(0.5*e*a2 + (c-0.75*e)*g);
  S_3232 = S_2323;
  S_1212 = 0.25*b*(c-(a2+1)*e-0.5*(c-3*e*(a2+1))*g);
  S_1313 = S_1212;
  S_3131 = S_1313;

elseif (geom == 3)
  % Disc-shaped inclusions
  l = 0.5       % fibre length
  d = 1       % fibre diameter
  a = l/d     % aspect ratio
  a2 = power(a,2.0)
  g = (a/power(1-a2,1.5))*(acos(a)-a*sqrt(1-a2))
  b = 1/(1-nu_0)
  c = 1-2*nu_0
  e = 1/(a2-1)

  S_1111 = 0.5*b*(c + e*(3*a2-1)-(c+3*e*a2)*g);
  S_2222 = (3/8)*b*e*a2+0.25*b*(c-(9/4)*e)*g;
  S_3333 = S_2222;
  S_2233 = 0.25*b*(0.5*e*a2-(c+0.75*e)*g);
  S_3322 = S_2233;
  S_2211 = -0.5*b*e*a2 + 0.25*b*(3*e*a2-c)*g;
  S_3311 = S_2211;
  S_1122 = -0.5*b*(c+e)+0.5*b*(c+1.5*e)*g;
  S_1133 = S_1122;
  S_2323 = 0.25*b*(0.5*e*a2 + (c-0.75*e)*g);
  S_3232 = S_2323;
  S_1212 = 0.25*b*(c-(a2+1)*e-0.5*(c-3*e*(a2+1))*g);
  S_1313 = S_1212;
  S_3131 = S_1313;
```

```
end

% Eshelby tensor (using engineering strains)
S = zeros(6,6);

% Matrix form:
S(1,1) = S_1111;
S(1,2) = S_1122;
S(1,3) = S_1133;
S(2,1) = S_2211;
S(2,2) = S_2222;
S(2,3) = S_2233;
S(3,1) = S_3311;
S(3,2) = S_3322;
S(3,3) = S_3333;
S(4,4) = 2*S_1212;
S(5,5) = 2*S_2323;
S(6,6) = 2*S_3131;
S;

% Dilute matrix
I = zeros(6,6);
I(1,1) = 1.0;
I(2,2) = 1.0;
I(3,3) = 1.0;
I(4,4) = 1.0;
I(5,5) = 1.0;
I(6,6) = 1.0;
I;

A_dil = inv(I+S*inv(C)*(D-C))
Vf = 0.0:0.001:0.2;

for i =1:length(Vf)
  V0 =(1-Vf(i));
  A_0 = inv(V0*I + Vf(i)*A_dil);
  A_r = A_dil*A_0;
  C_comp = V0*C*A_0 + Vf(i)*D*A_r

  % Calculating the composite elastic stiffness
  if (geom == 1)
    % Isotropic material properties
    nu_c = C_comp(1,2)/(C_comp(1,1)+C_comp(1,2));
```

```
    E_c  = 2*C_comp(4,4)*(1+nu_c);
    E_11(i) = E_c/E_0;
  elseif (geom == 2)
    % Transversely isotropic proerties
    S_comp = inv(C_comp);
    E_11(i) = 1/(S_comp(1,1)*E_0);
  elseif (geom == 3)
    % Transversely isotropic proerties
    S_comp = inv(C_comp);
    E_11(i) = 1/(S_comp(1,1)*E_0);
  end
end

if (geom ==1)
  plot(Vf,E_11,'b')
elseif (geom == 2)
  plot(Vf,E_11,'c')
elseif (geom == 3)
  plot(Vf,E_11, 'r')
end
xlabel ('V_f')
ylabel('E_{comp}/E_m')
```

B.2 Interphase model for aligned inclusions

```
% Interphase model
% File name: “interphase_1.m”
% Generally: One type of isotropic inclusion with interface
% Three geometries:
% 1) aligned spherical inclusions
% 2) aligned fiber-like inclusions with aspect ratio
% 3) aligned disc-shaped inclusion with aspect ratio
%
% Author: Tom Thorvaldsen, FFI, January 2014

% Elastic properties – bulk matrix
E_0 = 3.0; % GPa
nu_0 = 0.35;

C = zeros (6,6);
const = (E_0*(1-nu_0))/((1+nu_0)*(1-2*nu_0));
C(1,1) = const;
C(1,2)= const*(nu_0/(1-nu_0));
C(1,3)= const*(nu_0/(1-nu_0));
```

```
C(2,1) = C(1,2);
C(2,2) = const;
C(2,3) = const*(nu_0/(1-nu_0));
C(3,1) = C(1,3);
C(3,2) = C(2,3);
C(3,3) = const;
C(4,4) = const*((1-2*nu_0)/(2*(1-nu_0)));
C(5,5) = const*((1-2*nu_0)/(2*(1-nu_0)));
C(6,6) = const*((1-2*nu_0)/(2*(1-nu_0)));
C;

% Elastic properties - particle inclusion
E_p = 70 %GPa ;
nu_p = 0.20;

D = zeros (6,6);
const = (E_p*(1-nu_p))/((1+nu_p)*(1-2*nu_p));
D(1,1) = const;
D(1,2)= const*(nu_p/(1-nu_p));
D(1,3)= const*(nu_p/(1-nu_p));
D(2,1) = D(1,2);
D(2,2) = const;
D(2,3) = const*(nu_p/(1-nu_p));
D(3,1) = D(1,3);
D(3,2) = D(2,3);
D(3,3) = const;
D(4,4) = const*((1-2*nu_p)/(2*(1-nu_p)));
D(5,5) = const*((1-2*nu_p)/(2*(1-nu_p)));
D(6,6) = const*((1-2*nu_p)/(2*(1-nu_p)));
D;

% Elastic properties  - interface
E_i = 4.0; %GPa
nu_i = 0.35;

H = zeros (6,6);
const = (E_i*(1-nu_i))/((1+nu_i)*(1-2*nu_i));
H(1,1) = const;
H(1,2)= const*(nu_i/(1-nu_i));
H(1,3)= const*(nu_i/(1-nu_i));
H(2,1) = H(1,2);
H(2,2) = const;
H(2,3) = const*(nu_i/(1-nu_i));
```

```
H(3,1) = H(1,3);
H(3,2) = H(2,3);
H(3,3) = const;
H(4,4) = const*((1-2*nu_i)/(2*(1-nu_i)));
H(5,5) = const*((1-2*nu_i)/(2*(1-nu_i)));
H(6,6) = const*((1-2*nu_i)/(2*(1-nu_i)));
H;

% Geometry:
geom = 1  % spherical inclusions
%geom = 2  % fiber-like inclusions
%geom = 3  % disc-shaped inclusions

if (geom == 1)
  % Spherical inclusions:
  S_1111 = (7-5*nu_0)/(15*(1-nu_0));
  S_2222 = S_1111;
  S_3333 = S_1111;
  S_1122 = (5*nu_0-1)/(15*(1-nu_0));
  S_1133 = S_1122;
  S_2211 = S_1122;
  S_2233 = S_1122;
  S_3311 = S_1122;
  S_3322 = S_1122;
  S_1212 = (4-5*nu_0)/(15*(1-nu_0));
  S_1221 = S_1212;
  S_2323 = S_1212;
  S_2332 = S_1212;
  S_3131 = S_1212;
  S_3113 = S_1212;

elseif (geom == 2)
  % Fiber-like inclusions:
  l = 3       % fibre length
  d = 1       % fibre diameter
  a = l/d     % aspect ratio
  a2 = power(a,2.0)
  g = (a/power(a2-1,1.5))*(a*sqrt(a2-1)-acosh(a))
  b = 1/(1-nu_0)
  c = 1-2*nu_0
  e = 1/(a2-1)

  S_1111 = 0.5*b*(c + e*(3*a2-1)-(c+3*e*a2)*g)
```

```
  S_2222 = (3/8)*b*e*a2+0.25*b*(c-(9/4)*e)*g;
  S_3333 = S_2222;
  S_2233 = 0.25*b*(0.5*e*a2-(c+0.75*e)*g);
  S_3322 = S_2233;
  S_2211 = -0.5*b*e*a2 + 0.25*b*(3*e*a2-c)*g;
  S_3311 = S_2211;
  S_1122 = -0.5*b*(c+e)+0.5*b*(c+1.5*e)*g;
  S_1133 = S_1122;
  S_2323 = 0.25*b*(0.5*e*a2 + (c-0.75*e)*g);
  S_3232 = S_2323;
  S_1212 = 0.25*b*(c-(a2+1)*e-0.5*(c-3*e*(a2+1))*g);
  S_1313 = S_1212;
  S_3131 = S_1313;

elseif (geom == 3)
  % Disc-shaped inclusions
  l = 1       % fibre length
  d = 3       % fibre diameter
  a = l/d     % aspect ratio
  a2 = power(a,2.0)
  g = (a/power(1-a2,1.5))*(acos(a)-a*sqrt(1-a2))
  b = 1/(1-nu_0)
  c = 1-2*nu_0
  e = 1/(a2-1)

  S_1111 = 0.5*b*(c + e*(3*a2-1)-(c+3*e*a2)*g);
  S_2222 = (3/8)*b*e*a2+0.25*b*(c-(9/4)*e)*g;
  S_3333 = S_2222;
  S_2233 = 0.25*b*(0.5*e*a2-(c+0.75*e)*g);
  S_3322 = S_2233;
  S_2211 = -0.5*b*e*a2 + 0.25*b*(3*e*a2-c)*g;
  S_3311 = S_2211;
  S_1122 = -0.5*b*(c+e)+0.5*b*(c+1.5*e)*g;
  S_1133 = S_1122;
  S_2323 = 0.25*b*(0.5*e*a2 + (c-0.75*e)*g);
  S_3232 = S_2323;
  S_1212 = 0.25*b*(c-(a2+1)*e-0.5*(c-3*e*(a2+1))*g);
  S_1313 = S_1212;
  S_3131 = S_1313;
end

% Eshelby tensor (using engineering strains)
S = zeros(6,6);
```

```
% Matrix form:
S(1,1) = S_1111;
S(1,2) = S_1122;
S(1,3) = S_1133;
S(2,1) = S_2211;
S(2,2) = S_2222;
S(2,3) = S_2233;
S(3,1) = S_3311;
S(3,2) = S_3322;
S(3,3) = S_3333;
S(4,4) = 2*S_1212;
S(5,5) = 2*S_2323;
S(6,6) = 2*S_3131;
S;

% Dilute matrix
I = zeros(6,6);
I(1,1) = 1.0;
I(2,2) = 1.0;
I(3,3) = 1.0;
I(4,4) = 1.0;
I(5,5) = 1.0;
I(6,6) = 1.0;
I;

J = inv(S+inv(D-C)*C)
K = inv(S+inv(H-C)*C)
A_p = I-S*J

n = 1.5  % Size of interphase; r_i = n*r_p
Vf = 0.0:0.001:0.20;
E_11(1) = 1.0 % to avoid dividing on zero in the expressions in the for-
loop

for j =2:length(Vf)
  Vi = (n^3-1)*Vf(j)  % volume fraction of the interface; function of Vf
  V0 =(1-Vf(j)-Vi);
  if (V0>=0.0)
    A_pi = I-S*((Vf(j)/(Vf(j)+Vi))*J+(Vi/(Vf(j)+Vi))*K)
    C_comp = C +((Vf(j)+Vi)*(H-C)*A_pi+Vf(j)*(D-H)*A_p)*inv(V0*I...
         +(Vf(j)+Vi)*A_pi)

    if (geom == 1)
```

```
      % Isotropic material properties
      nu_c = C_comp(1,2)/(C_comp(1,1)+C_comp(1,2));
      E_c  = 2*C_comp(4,4)*(1+nu_c);
      E_11(j) = E_c/E_0;
    elseif (geom == 2)
      % Transversely isotropic properties
      S_comp = inv(C_comp);
      E_11(j) = 1/(S_comp(1,1)*E_0);
    elseif (geom == 3)
      % Transversely isotropic properties
      S_comp = inv(C_comp);
      E_11(j) = 1/(S_comp(1,1)*E_0);
    end
  else
    E_11(j)=0.0;
  end
end

if (geom ==1)
  plot(Vf,E_11,'b')
elseif (geom == 2)
  plot(Vf,E_11,'g')
elseif (geom == 3)
  plot(Vf,E_11, 'g')
end
xlabel ('V_f')
ylabel('E_{comp}/E_m')
```

B.3 General Mori-Tanaka model for randomly oriented inclusions

```
% Mori-Tanaka – general model
% File name: “mori_tanaka_6.m”
% Generally: Model N-1 spheroid shaped inclusions in an
% isotropic matrix
% This case: One type of isotropic inclusion
% Three geometries:
% 1) random spherical inclusions
% 2) random fibre-like inclusions with aspect ratio
% 3) random disc-shaped inclusion with aspect ratio
%
% Author: Tom Thorvaldsen, FFI, March 2014

% Elastic parameters - matrix
E_0 = 3.12
```

```
nu_0 = 0.35

C = zeros (6,6);
const = (E_0*(1-nu_0))/((1+nu_0)*(1-2*nu_0));
C(1,1) = const;
C(1,2)= const*(nu_0/(1-nu_0));
C(1,3)= const*(nu_0/(1-nu_0));
C(2,1) = C(1,2);
C(2,2) = const;
C(2,3) = const*(nu_0/(1-nu_0));
C(3,1) = C(1,3);
C(3,2) = C(2,3);
C(3,3) = const;
C(4,4) = const*((1-2*nu_0)/(2*(1-nu_0)));
C(5,5) = const*((1-2*nu_0)/(2*(1-nu_0)));
C(6,6) = const*((1-2*nu_0)/(2*(1-nu_0)));
C;

% Elastic parameters - inclusion
E_i = 386
nu_i = 0.22

D = zeros (6,6);
const = (E_i*(1-nu_i))/((1+nu_i)*(1-2*nu_i));
D(1,1) = const;
D(1,2)= const*(nu_i/(1-nu_i));
D(1,3)= const*(nu_i/(1-nu_i));
D(2,1) = D(1,2);
D(2,2) = const;
D(2,3) = const*(nu_i/(1-nu_i));
D(3,1) = D(1,3);
D(3,2) = D(2,3);
D(3,3) = const;
D(4,4) = const*((1-2*nu_i)/(2*(1-nu_i)));
D(5,5) = const*((1-2*nu_i)/(2*(1-nu_i)));
D(6,6) = const*((1-2*nu_i)/(2*(1-nu_i)));
D;

% Geometry:
geom = 1  % spherical inclusions
%geom = 2  % fibre-like inclusions
%geom = 3  % disc-shaped inclusions
```

```
if (geom == 1)
  % Spherical inclusions:
  S_1111 = (7-5*nu_0)/(15*(1-nu_0));
  S_2222 = S_1111
  S_3333 = S_1111
  S_1122 = (5*nu_0-1)/(15*(1-nu_0));
  S_1133 = S_1122
  S_2211 = S_1122
  S_2233 = S_1122
  S_3311 = S_1122
  S_3322 = S_1122
  S_1212 = (4-5*nu_0)/(15*(1-nu_0))
  S_1221 = S_1212
  S_2323 = S_1212
  S_2332 = S_1212
  S_3131 = S_1212
  S_3113 = S_1212

elseif (geom == 2)
  % Fiber-like inclusions:
  l = 1000      % fibre length
  d = 1       % fibre diameter
  a = l/d     % aspect ratio
  a2 = power(a,2.0)
  g = (a/power(a2-1,1.5))*(a*sqrt(a2-1)-acosh(a))
  b = 1/(1-nu_0)
  c = 1-2*nu_0
  e = 1/(a2-1)

  S_1111 = 0.5*b*(c + e*(3*a2-1)-(c+3*e*a2)*g)
  S_2222 = (3/8)*b*e*a2+0.25*b*(c-(9/4)*e)*g;
  S_3333 = S_2222;
  S_2233 = 0.25*b*(0.5*e*a2-(c+0.75*e)*g);
  S_3322 = S_2233;
  S_2211 = -0.5*b*e*a2 + 0.25*b*(3*e*a2-c)*g;
  S_3311 = S_2211;
  S_1122 = -0.5*b*(c+e)+0.5*b*(c+1.5*e)*g;
  S_1133 = S_1122;
  S_2323 = 0.25*b*(0.5*e*a2 + (c-0.75*e)*g);
  S_3232 = S_2323;
  S_1212 = 0.25*b*(c-(a2+1)*e-0.5*(c-3*e*(a2+1))*g);
  S_1313 = S_1212;
  S_3131 = S_1313;
```

```
elseif (geom == 3)
  % Disc-shaped inclusions
  l = 0.00005       % fibre length
  d = 1       % fibre diameter
  a = l/d     % aspect ratio
  a2 = power(a,2.0)
  g = (a/power(1-a2,1.5))*(acos(a)-a*sqrt(1-a2))
  b = 1/(1-nu_0)
  c = 1-2*nu_0
  e = 1/(a2-1)

  S_1111 = 0.5*b*(c + e*(3*a2-1)-(c+3*e*a2)*g);
  S_2222 = (3/8)*b*e*a2+0.25*b*(c-(9/4)*e)*g;
  S_3333 = S_2222;
  S_2233 = 0.25*b*(0.5*e*a2-(c+0.75*e)*g);
  S_3322 = S_2233;
  S_2211 = -0.5*b*e*a2 + 0.25*b*(3*e*a2-c)*g;
  S_3311 = S_2211;
  S_1122 = -0.5*b*(c+e)+0.5*b*(c+1.5*e)*g;
  S_1133 = S_1122;
  S_2323 = 0.25*b*(0.5*e*a2 + (c-0.75*e)*g);
  S_3232 = S_2323;
  S_1212 = 0.25*b*(c-(a2+1)*e-0.5*(c-3*e*(a2+1))*g);
  S_1313 = S_1212;
  S_3131 = S_1313;
end

% Eshelby tensor (using engineering strains)
S = zeros(6,6);
% Matrix form:
S(1,1) = S_1111;
S(1,2) = S_1122;
S(1,3) = S_1133;
S(2,1) = S_2211;
S(2,2) = S_2222;
S(2,3) = S_2233;
S(3,1) = S_3311;
S(3,2) = S_3322;
S(3,3) = S_3333;
S(4,4) = 2*S_1212;
S(5,5) = 2*S_2323;
S(6,6) = 2*S_3131;
S;
```

```
% Dilute matrix
I = zeros(6,6);
I(1,1) = 1.0;
I(2,2) = 1.0;
I(3,3) = 1.0;
I(4,4) = 1.0;
I(5,5) = 1.0;
I(6,6) = 1.0;
I;

A_dil = inv(I+S*inv(C)*(D-C))

% Averaging matrix
M =(1/120)*[24 64 0 16 16 0 0 0 0 0 0 64;
  24 9 45 6 6 10 10 5 5 20 40 24;
  24 9 45 6 6 10 10 5 5 20 40 24;
  8 8 0 12 32 20 0 40 0 0 0 -32;
  8 8 0 32 12 0 20 0 40 0 0 -32;
  8 8 0 12 32 20 0 40 0 0 0 -32;
  8 8 0 32 12 0 20 0 40 0 0 -32;
  8 3 15 2 2 30 30 15 15 -20 -40 8;
  8 3 15 2 2 30 30 15 15 -20 -40 8;
  8 3 15 2 2 -10 -10 -5 -5 20 40 8;
  8 8 0 -8 -8 0 0 0 0 40 20 28;
  8 8 0 -8 -8 0 0 0 0 40 20 28]

D_A_dil = D*A_dil

% Averaging of D_A_dil
D_A_dil_vec(1) = D_A_dil(1,1);
D_A_dil_vec(2) = D_A_dil(2,2);
D_A_dil_vec(3) = D_A_dil(3,3);
D_A_dil_vec(4) = D_A_dil(1,2);
D_A_dil_vec(5) = D_A_dil(2,1);
D_A_dil_vec(6) = D_A_dil(1,3);
D_A_dil_vec(7) = D_A_dil(3,1);
D_A_dil_vec(8) = D_A_dil(2,3);
D_A_dil_vec(9) = D_A_dil(3,2);
D_A_dil_vec(10) = D_A_dil(4,4);
D_A_dil_vec(11) = D_A_dil(5,5);
D_A_dil_vec(12) = D_A_dil(6,6);

D_A_dil_aver_vec = M*transpose(D_A_dil_vec);
```

```
D_A_dil_aver(1,1) = D_A_dil_aver_vec(1);
D_A_dil_aver(2,2) = D_A_dil_aver_vec(2);
D_A_dil_aver(3,3) = D_A_dil_aver_vec(3);
D_A_dil_aver(1,2) = D_A_dil_aver_vec(4);
D_A_dil_aver(2,1) = D_A_dil_aver_vec(5);
D_A_dil_aver(1,3) = D_A_dil_aver_vec(6);
D_A_dil_aver(3,1) = D_A_dil_aver_vec(7);
D_A_dil_aver(2,3) = D_A_dil_aver_vec(8);
D_A_dil_aver(3,2) = D_A_dil_aver_vec(9);
D_A_dil_aver(4,4) = D_A_dil_aver_vec(10);
D_A_dil_aver(5,5) = D_A_dil_aver_vec(11);
D_A_dil_aver(6,6) = D_A_dil_aver_vec(12);
D_A_dil_aver;

% Averaging of A_dil
A_dil_vec(1) = A_dil(1,1);
A_dil_vec(2) = A_dil(2,2);
A_dil_vec(3) = A_dil(3,3);
A_dil_vec(4) = A_dil(1,2);
A_dil_vec(5) = A_dil(2,1);
A_dil_vec(6) = A_dil(1,3);
A_dil_vec(7) = A_dil(3,1);
A_dil_vec(8) = A_dil(2,3);
A_dil_vec(9) = A_dil(3,2);
A_dil_vec(10) = A_dil(4,4);
A_dil_vec(11) = A_dil(5,5);
A_dil_vec(12) = A_dil(6,6);

A_dil_aver_vec = M*transpose(A_dil_vec);

A_dil_aver(1,1) = A_dil_aver_vec(1);
A_dil_aver(2,2) = A_dil_aver_vec(2);
A_dil_aver(3,3) = A_dil_aver_vec(3);
A_dil_aver(1,2) = A_dil_aver_vec(4);
A_dil_aver(2,1) = A_dil_aver_vec(5);
A_dil_aver(1,3) = A_dil_aver_vec(6);
A_dil_aver(3,1) = A_dil_aver_vec(7);
A_dil_aver(2,3) = A_dil_aver_vec(8);
A_dil_aver(3,2) = A_dil_aver_vec(9);
A_dil_aver(4,4) = A_dil_aver_vec(10);
A_dil_aver(5,5) = A_dil_aver_vec(11);
A_dil_aver(6,6) = A_dil_aver_vec(12);
A_dil_aver;
```

```
Vf = 0.0:0.001:0.2;
for i =1:length(Vf)
  V0 =(1-Vf(i));
  if (geom == 1)
    A_0 = inv(V0*I + Vf(i)*A_dil);   % gives the correct spherical
distr.
  elseif (geom == 2)
    A_0 = inv(V0*I + Vf(i)*A_dil_aver); % gives a transversely iso
C_comp
  elseif (geom == 3)
    A_0 = inv(V0*I + Vf(i)*A_dil_aver);
  end

  C_comp = (V0*C + Vf(i)*D_A_dil_aver)*A_0

  if (geom == 1)
    % Isotropic material properties
    nu_c = C_comp(1,2)/(C_comp(1,1)+C_comp(1,2));
    E_c  = 2*C_comp(4,4)*(1+nu_c);
    E_11(i) = E_c/E_0;
  elseif (geom == 2)
    % Transversely isotropic properties
    S_comp = inv(C_comp);
    E_11(i) = 1/(S_comp(1,1)*E_0);
  elseif (geom == 3)
    % Transversely isotropic proerties%
    S_comp = inv(C_comp);
    E_11(i) = 1/(S_comp(1,1)*E_0);
  end
end

if (geom ==1)
  plot(Vf,E_11,'r')
elseif (geom == 2)
  plot(Vf,E_11, 'c')
elseif (geom == 3)
  plot(Vf,E_11, 'r--')
end
xlabel ('V_f')
ylabel('E_{comp}/E_0')
```

B.4 Interphase model for random oriented inclusions

```
% Interface model
% File name: “interphase_2.m”
% Generally: One type of isotropic inclusion with interface
% Three geometries:
% 1) random spherical inclusions
% 2) random fiber-like inclusions with aspect ratio
% 3) random disc-shaped inclusion with aspect ratio
% Author: Tom Thorvaldsen, FFI, January 2014
% Elastic properties – bulk matrix
E_0 = 3.0; % GPa
nu_0 = 0.35;

C = zeros (6,6);
const = (E_0*(1-nu_0))/((1+nu_0)*(1-2*nu_0));
C(1,1) = const;
C(1,2)= const*(nu_0/(1-nu_0));
C(1,3)= const*(nu_0/(1-nu_0));
C(2,1) = C(1,2);
C(2,2) = const;
C(2,3) = const*(nu_0/(1-nu_0));
C(3,1) = C(1,3);
C(3,2) = C(2,3);
C(3,3) = const;
C(4,4) = const*((1-2*nu_0)/(2*(1-nu_0)));
C(5,5) = const*((1-2*nu_0)/(2*(1-nu_0)));
C(6,6) = const*((1-2*nu_0)/(2*(1-nu_0)));
C;

% Elastic propeties - particle inclusion
E_p = 70; %GPa ;
nu_p = 0.20;

D = zeros (6,6);
const = (E_p*(1-nu_p))/((1+nu_p)*(1-2*nu_p));
D(1,1) = const;
D(1,2)= const*(nu_p/(1-nu_p));
D(1,3)= const*(nu_p/(1-nu_p));
D(2,1) = D(1,2);
D(2,2) = const;
D(2,3) = const*(nu_p/(1-nu_p));
D(3,1) = D(1,3);
D(3,2) = D(2,3);
```

```
D(3,3) = const;
D(4,4) = const*((1-2*nu_p)/(2*(1-nu_p)));
D(5,5) = const*((1-2*nu_p)/(2*(1-nu_p)));
D(6,6) = const*((1-2*nu_p)/(2*(1-nu_p)));
D;

% Elastic propeties  - interface
E_i = 4.0 %386 %GPa ;
nu_i = 0.35 % 0.22 % 0.2;

H = zeros (6,6);
const = (E_i*(1-nu_i))/((1+nu_i)*(1-2*nu_i));
H(1,1) = const;
H(1,2)= const*(nu_i/(1-nu_i));
H(1,3)= const*(nu_i/(1-nu_i));
H(2,1) = H(1,2);
H(2,2) = const;
H(2,3) = const*(nu_i/(1-nu_i));
H(3,1) = H(1,3);
H(3,2) = H(2,3);
H(3,3) = const;
H(4,4) = const*((1-2*nu_i)/(2*(1-nu_i)));
H(5,5) = const*((1-2*nu_i)/(2*(1-nu_i)));
H(6,6) = const*((1-2*nu_i)/(2*(1-nu_i)));
H;

% Geometry:
%geom = 1  % spherical inclusions
%geom = 2  % fiber-like inclusions
geom = 3  % disc-shaped inclusions

if (geom == 1)
  % Spherical inclusions:
  S_1111 = (7-5*nu_0)/(15*(1-nu_0));
  S_2222 = S_1111;
  S_3333 = S_1111;
  S_1122 = (5*nu_0-1)/(15*(1-nu_0));
  S_1133 = S_1122;
  S_2211 = S_1122;
  S_2233 = S_1122;
  S_3311 = S_1122;
  S_3322 = S_1122;
  S_1212 = (4-5*nu_0)/(15*(1-nu_0));
```

```
  S_1221 = S_1212;
  S_2323 = S_1212;
  S_2332 = S_1212;
  S_3131 = S_1212;
  S_3113 = S_1212;

elseif (geom == 2)
  % Fiber-like inclusions:
  l = 3.0       % fibre length
  d = 1.0       % fibre diameter
  a = l/d     % aspect ratio
  a2 = power(a,2.0)
  g = (a/power(a2-1,1.5))*(a*sqrt(a2-1)-acosh(a))
  b = 1/(1-nu_0)
  c = 1-2*nu_0
  e = 1/(a2-1)

  S_1111 = 0.5*b*(c + e*(3*a2-1)-(c+3*e*a2)*g)
  S_2222 = (3/8)*b*e*a2+0.25*b*(c-(9/4)*e)*g;
  S_3333 = S_2222;
  S_2233 = 0.25*b*(0.5*e*a2-(c+0.75*e)*g);
  S_3322 = S_2233;
  S_2211 = -0.5*b*e*a2 + 0.25*b*(3*e*a2-c)*g;
  S_3311 = S_2211;
  S_1122 = -0.5*b*(c+e)+0.5*b*(c+1.5*e)*g;
  S_1133 = S_1122;
  S_2323 = 0.25*b*(0.5*e*a2 + (c-0.75*e)*g);
  S_3232 = S_2323;
  S_1212 = 0.25*b*(c-(a2+1)*e-0.5*(c-3*e*(a2+1))*g);
  S_1313 = S_1212;
  S_3131 = S_1313;

elseif (geom == 3)
  % Disc-shaped inclusions
  l = 1.0       % fibre length
  d = 3.0       % fibre diameter
  a = l/d     % aspect ratio
  a2 = power(a,2.0)
  g = (a/power(1-a2,1.5))*(acos(a)-a*sqrt(1-a2))
  b = 1/(1-nu_0)
  c = 1-2*nu_0
  e = 1/(a2-1)
```

```
  S_1111 = 0.5*b*(c + e*(3*a2-1)-(c+3*e*a2)*g);
  S_2222 = (3/8)*b*e*a2+0.25*b*(c-(9/4)*e)*g;
  S_3333 = S_2222;
  S_2233 = 0.25*b*(0.5*e*a2-(c+0.75*e)*g);
  S_3322 = S_2233;
  S_2211 = -0.5*b*e*a2 + 0.25*b*(3*e*a2-c)*g;
  S_3311 = S_2211;
  S_1122 = -0.5*b*(c+e)+0.5*b*(c+1.5*e)*g;
  S_1133 = S_1122;
  S_2323 = 0.25*b*(0.5*e*a2 + (c-0.75*e)*g);
  S_3232 = S_2323;
  S_1212 = 0.25*b*(c-(a2+1)*e-0.5*(c-3*e*(a2+1))*g);
  S_1313 = S_1212;
  S_3131 = S_1313;
end

% Eshelby tensor (using engineering strains)
S = zeros(6,6);
% Matrix form:
S(1,1) = S_1111;
S(1,2) = S_1122;
S(1,3) = S_1133;
S(2,1) = S_2211;
S(2,2) = S_2222;
S(2,3) = S_2233;
S(3,1) = S_3311;
S(3,2) = S_3322;
S(3,3) = S_3333;
S(4,4) = 2*S_1212;
S(5,5) = 2*S_2323;
S(6,6) = 2*S_3131;
S;

% Dilute matrix
I = zeros(6,6);
I(1,1) = 1.0;
I(2,2) = 1.0;
I(3,3) = 1.0;
I(4,4) = 1.0;
I(5,5) = 1.0;
I(6,6) = 1.0;
I;
```

```
J = inv(S+inv(D-C)*C)
K = inv(S+inv(H-C)*C)

A_p = I-S*J

% Average matrix
M =(1/120)*[24 64 0 16 16 0 0 0 0 0 0 64;
  24 9 45 6 6 10 10 5 5 20 40 24;
  24 9 45 6 6 10 10 5 5 20 40 24;
  8 8 0 12 32 20 0 40 0 0 0 -32;
  8 8 0 32 12 0 20 0 40 0 0 -32;
  8 8 0 12 32 20 0 40 0 0 0 -32;
 8 8 0 32 12 0 20 0 40 0 0 -32;
  8 3 15 2 2 30 30 15 15 -20 -40 8;
  8 3 15 2 2 30 30 15 15 -20 -40 8;
  8 3 15 2 2 -10 -10 -5 -5 20 40 8;
  8 8 0 -8 -8 0 0 0 0 40 20 28;
  8 8 0 -8 -8 0 0 0 0 40 20 28]

DH_Ap = (D-H)*A_p

% Averaging of DH_Ap
DH_Ap_vec(1) = DH_Ap(1,1);
DH_Ap_vec(2) = DH_Ap(2,2);
DH_Ap_vec(3) = DH_Ap(3,3);
DH_Ap_vec(4) = DH_Ap(1,2);
DH_Ap_vec(5) = DH_Ap(2,1);
DH_Ap_vec(6) = DH_Ap(1,3);
DH_Ap_vec(7) = DH_Ap(3,1);
DH_Ap_vec(8) = DH_Ap(2,3);
DH_Ap_vec(9) = DH_Ap(3,2);
DH_Ap_vec(10) = DH_Ap(4,4);
DH_Ap_vec(11) = DH_Ap(5,5);
DH_Ap_vec(12) = DH_Ap(6,6);

DH_Ap_aver_vec = M*transpose(DH_Ap_vec);

DH_Ap_aver(1,1) = DH_Ap_aver_vec(1);
DH_Ap_aver(2,2) = DH_Ap_aver_vec(2);
DH_Ap_aver(3,3) = DH_Ap_aver_vec(3);
DH_Ap_aver(1,2) = DH_Ap_aver_vec(4);
DH_Ap_aver(2,1) = DH_Ap_aver_vec(5);
DH_Ap_aver(1,3) = DH_Ap_aver_vec(6);
```

```
DH_Ap_aver(3,1) = DH_Ap_aver_vec(7);
DH_Ap_aver(2,3) = DH_Ap_aver_vec(8);
DH_Ap_aver(3,2) = DH_Ap_aver_vec(9);
DH_Ap_aver(4,4) = DH_Ap_aver_vec(10);
DH_Ap_aver(5,5) = DH_Ap_aver_vec(11);
DH_Ap_aver(6,6) = DH_Ap_aver_vec(12);

DH_Ap_aver;

n = 1.5  % r_i = n*r_p
Vf = 0.0:0.001:0.2;
E_11(1) = 1.0

for j =2:length(Vf)
  Vi = (n^3-1)*Vf(j)  % volume fraction of the interface; function of Vf
  V0 =(1-Vf(j)-Vi);
  if (V0>=0.0)
    A_pi = I-S*((Vf(j)/(Vf(j)+Vi))*J+(Vi/(Vf(j)+Vi))*K)

    % Averaging of A_pi
    Api_vec(1) = A_pi(1,1);
    Api_vec(2) = A_pi(2,2);
    Api_vec(3) = A_pi(3,3);
    Api_vec(4) = A_pi(1,2);
    Api_vec(5) = A_pi(2,1);
    Api_vec(6) = A_pi(1,3);
    Api_vec(7) = A_pi(3,1);
    Api_vec(8) = A_pi(2,3);
    Api_vec(9) = A_pi(3,2);
    Api_vec(10) = A_pi(4,4);
    Api_vec(11) = A_pi(5,5);
    Api_vec(12) = A_pi(6,6);

    Api_aver_vec = M*transpose(Api_vec);

    Api_aver(1,1) = Api_aver_vec(1);
    Api_aver(2,2) = Api_aver_vec(2);
    Api_aver(3,3) = Api_aver_vec(3);
    Api_aver(1,2) = Api_aver_vec(4);
    Api_aver(2,1) = Api_aver_vec(5);
    Api_aver(1,3) = Api_aver_vec(6);
    Api_aver(3,1) = Api_aver_vec(7);
    Api_aver(2,3) = Api_aver_vec(8);
```

```
    Api_aver(3,2) = Api_aver_vec(9);
    Api_aver(4,4) = Api_aver_vec(10);
    Api_aver(5,5) = Api_aver_vec(11);
    Api_aver(6,6) = Api_aver_vec(12);

    Api_aver;

    % Averaging of HC_Api
    HC_Api = (H-C)*A_pi

    HC_Api_vec(1) = HC_Api(1,1);
    HC_Api_vec(2) = HC_Api(2,2);
  HC_Api_vec(3) = HC_Api(3,3);
    HC_Api_vec(4) = HC_Api(1,2);
    HC_Api_vec(5) = HC_Api(2,1);
    HC_Api_vec(6) = HC_Api(1,3);
    HC_Api_vec(7) = HC_Api(3,1);
    HC_Api_vec(8) = HC_Api(2,3);
    HC_Api_vec(9) = HC_Api(3,2);
    HC_Api_vec(10) = HC_Api(4,4);
    HC_Api_vec(11) = HC_Api(5,5);
    HC_Api_vec(12) = HC_Api(6,6);

    HC_Api_aver_vec = M*transpose(HC_Api_vec);

    HC_Api_aver(1,1) = HC_Api_aver_vec(1);
    HC_Api_aver(2,2) = HC_Api_aver_vec(2);
    HC_Api_aver(3,3) = HC_Api_aver_vec(3);
    HC_Api_aver(1,2) = HC_Api_aver_vec(4);
    HC_Api_aver(2,1) = HC_Api_aver_vec(5);
    HC_Api_aver(1,3) = HC_Api_aver_vec(6);
    HC_Api_aver(3,1) = HC_Api_aver_vec(7);
    HC_Api_aver(2,3) = HC_Api_aver_vec(8);
    HC_Api_aver(3,2) = HC_Api_aver_vec(9);
    HC_Api_aver(4,4) = HC_Api_aver_vec(10);
    HC_Api_aver(5,5) = HC_Api_aver_vec(11);
    HC_Api_aver(6,6) = HC_Api_aver_vec(12);

    HC_Api_aver;

    if (geom == 1)
      A_0 = inv(V0*I+(Vf(j)+Vi)*A_pi);   % Gives the correct spherical
distr.
```

```
    elseif (geom == 2)
      A_0 = inv(V0*I+(Vf(j)+Vi)*Api_aver); % gives a transversely iso
C_comp
    elseif (geom == 3)
      A_0 = inv(V0*I+(Vf(j)+Vi)*Api_aver);
    end

    C_comp = C +((Vf(j)+Vi)*HC_Api_aver+Vf(j)*DH_Ap_aver)*A_0

    if (geom == 1)
      % Isotropic material properties
      nu_c = C_comp(1,2)/(C_comp(1,1)+C_comp(1,2));
      E_c  = 2*C_comp(4,4)*(1+nu_c);
      E_11(j) = E_c/E_0;
    elseif (geom == 2)
      % Transversely isotropic properties
      S_comp = inv(C_comp);
      E_11(j) = 1/(S_comp(1,1)*E_0);
    elseif (geom == 3)
      % Transversely isotropic proerties
      S_comp = inv(C_comp);
      E_11(j) = 1/(S_comp(1,1)*E_0);
    end
  else
    E_11(j)=0.0;
  end
end


if (geom ==1)
  plot(Vf,E_11,'c')
elseif (geom == 2)
  plot(Vf,E_11,'r')
elseif (geom == 3)
  plot(Vf,E_11, 'r')
end
xlabel ('V_f')
ylabel('E_{comp}/E_m')
```

References

[1] T. Thorvaldsen, "Modelling the elastic stiffness of nanocomposites using the Mori-Tanaka method ," Forsvarets forskningsinstitutt, FFI report 2015/00494 (Ugradert), 2015.

[2] T. Thorvaldsen, "Modelling the elastic stiffness of nanocomposites using three-phase models," FFI report 2005/00534 (Ugradert), 2015.

[3] F. Fisher and L. C. Brinson, "Nanomechanics of nanoreinforced polymers," in *Handbook of theoretical and computational nanotechnology: Functional nanomaterials, nanoparticles, and polymer design*. M. Rieth and W. Schommers, Eds. American Scientific Publishers, 2006, pp. 253-360.

[4] F. Bondioli, V. Cannillo, E. Fabbri, and M. Messori, "Epoxy-silica nanocomposites: preparation, experimental characterization, and modeling," *Journal of Applied Polymer Science*, vol. 97, no. 6, pp. 2382-2386, 2005.

[5] J. N. Coleman, U. Khan, W. J. Blau, and Y. K. Gun'ko, "Small but strong: A review of the mechanical properties of carbon nanotube-polymer composites," *Carbon*, vol. 44, no. 9, pp. 1624-1652, 2006.

[6] T. H. Hsieh, A. J. Kinloch, K. Masania, A. C. Taylor, and S. Sprenger, "The mechanisms and mechanics of the toughening of epoxy polymers modified with silica nanoparticles," *Polymer*, vol. 51, no. 26, pp. 6284-6294, 2010.

[7] T. Thorvaldsen, B. B. Johnsen, T. Olsen, and F. K. Hansen, "Investigation of theoretical models for the elastic stiffness of nanopaticle-modified polymer composites," *submitted to Nanocomposites*, 2015.

[8] J. D. Eshelby, "Elastic inclusions and inhomogeneities," in *Progress in Solid Mechanics*, 2nd ed. I. N. Sneddon and R. Hill, Eds. Amsterdam: North-Holland, 1961, pp. 89-140.

[9] J. D. Eshelby, "The determination of the elastic field of an ellipsoidal inclusion, and related problems," *Proceedings of the Royal Society of London*, vol. A241, no. 1226, pp. 376-396, 1957.

[10] M. L. Dunn and H. Ledbetter, "Elastic moduli of composites reinforced by multiphase particles," *Journal of Applied Mechanics*, vol. 62, no. 4, pp. 1023-1028, 1995.

[11] G. M. Odegard, T. C. Clancy, and T. S. Gates, "Modeling of the mechanical properties of nanoparticle/polymer composites," *Polymer*, vol. 46, no. 2, pp. 553-562, 2005.

[12] B. B. Johnsen, T. R. Frømyr, T. Thorvaldsen, and T. Olsen, "Preparation and characterisation of epoxy/alumina polymer nanocomposites," *Composite Interfaces*, vol. 20, no. 9, pp. 721-740, 2013.

[13] B. B. Johnsen, A. J. Kinloch, R. D. Mohammed, A. C. Taylor, and S. Sprenger, "Toughening mechanisms of nanoparticle-modified epoxy polymers," *Polymer*, vol. 48, no. 2, pp. 530-541, 2007.

[14] G. P. Tandon and G. J. Weng, "The effect of aspect ratio of inclusions on the elastic properties of unidirectionally aligned composites," *Polymer Composites*, vol. 5, no. 4, pp. 327-333, 1984.

[15] G. P. Tandon and G. J. Weng, "Average stress in the matrix and effective moduli of randomly oriented composites," *Composites Science and Technology,* vol. 27, no. 2, pp. 111-132, 1986.